#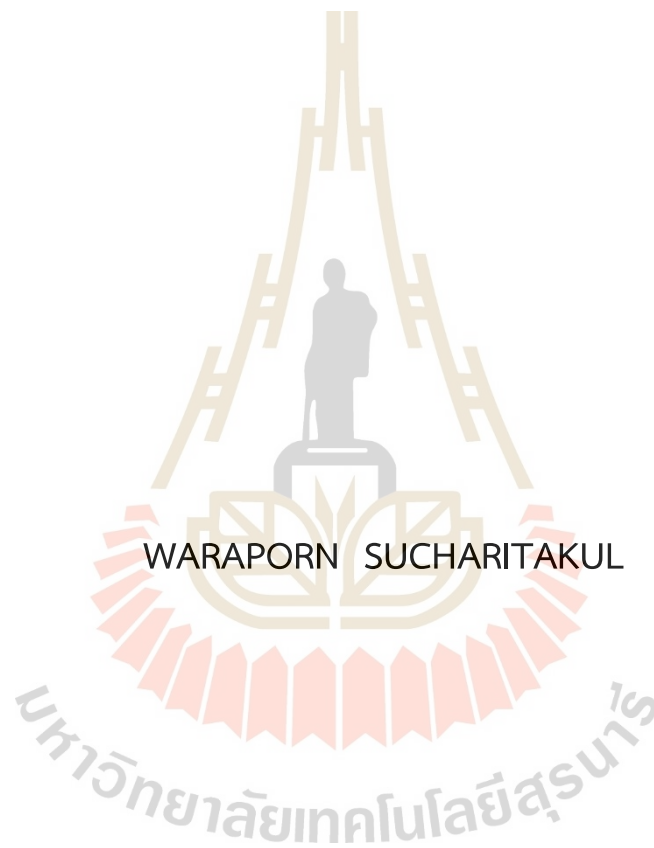 DETECTION OF ACETONE USING SI DOPED WO$_3$ NANORODS BASED GAS SENSORS PREPARED BY MAGNETRON SPUTTERING FOR DIABETES DIAGNOSIS

WARAPORN  SUCHARITAKUL

A Thesis Submitted in Partial Fulfilment of the Requirements for the

Degree of Master of Biomedical Innovation Engineering

Suranaree University of Technology

Academic Year 2021

การวินิจฉัยโรคเบาหวานจากการวัดระดับอะซิโตนโดยใช้แท่งนาโนทังสเตน
ไตรออกไซด์เจือซิลิกอนเตรียมด้วยเทคนิคการเคลือบฟิล์มบาง
แบบแมกนีตรอนสปัตเตอริงค์

นางสาววราภรณ์ สุจริตกุล

วิทยานิพนธ์นี้เป็นส่วนหนึ่งของการศึกษาตามหลักสูตรปริญญาวิศวกรรมศาสตรมหาบัณฑิต
สาขาวิชานวัตกรรม วิศวชีวการแพทย์
มหาวิทยาลัยเทคโนโลยีสุรนารี
ปีการศึกษา 2564

# DETECTION OF ACETONE USING SI DOPED WO$_3$ NANORODS BASED GAS SENSORS PREPARED BY MAGNETRON SPUTTERING FOR DIABETES DIAGNOSIS

Suranaree University of Technology has approved this thesis submitted in partial fulfillment of the requirements for a Master's Degree.

Thesis Examining Committee

_____
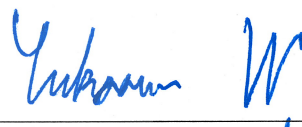
(Asst. Prof. Dr. Sukasem  Watcharamaisakul)

Chairperson

_____

(Asst. Prof. Dr. Pusit  Mitsomwang)

Member (Thesis Advisor)

_____

(Dr. Pattanaphong  Janphuang)

Member

_____

(Assoc. Prof. Dr. Chatchai  Jothityangkoon)

Vice Rector for Academic Affairs

and Quality Assurance

_____

(Assoc. Prof. Dr. Pornsiri  Jongkol)

Dean of Institute of Engineering

วราภรณ์ สุจริตกุล : การวินิจฉัยโรคเบาหวานจากการวัดระดับอะซิโตนโดยใช้แท่งนาโน
ทังสเตนไตรออกไซด์เจือซิลิกอนเตรียมด้วยเทคนิคการเคลือบฟิล์มบางแบบแมกนีตรอน
สปัตเตอริงค์ (DETECTION OF ACETONE USING SI DOPED WO₃ NANORODS BASED
GAS SENSORS PREPARED BY MAGNETRON SPUTTERING FOR DIABETES
DIAGNOSIS) อาจารย์ที่ปรึกษา : ผู้ช่วยศาสตราจารย์ ดร.ภูษิต มิตรสมหวัง, 51 หน้า.

คำสำคัญ: แท่งนาโนทังสเตนไตรออกไซด์เจือซิลิกอน/เซนเซอร์/อะซิโตน

ปัจจุบันเทคโนโลยีการตรวจจับก๊าซถูกนำไปใช้ในการใช้งานที่หลากหลาย ในการใช้งานทาง
การแพทย์ เซ็นเซอร์ตรวจจับก๊าซสามารถใช้ในการตรวจหาและวินิจฉัยโรคต่าง ๆ ที่มาจากความ
ผิดปกติของการเผาผลาญ เบาหวาน โรคหอบหืด ไต โรคตับ และมะเร็งปอด ในการศึกษานี้ ได้
ทำการศึกษาเซ็นเซอร์ตรวจจับก๊าซอะซิโตน โดยใช้วัสดุสารกึ่งตัวนำ แท่งนาโนทังสเตนไตรออกไซด์
เจือซิลิกอนที่เตรียมด้วยเทคนิคการเคลือบฟิล์มบางแบบแมกนีตรอนสปัตเตอริงค์ ด้วยเทคนิคการตก
สะสมมุมเฉียง (OAD) อัตราส่วนการเจือซิลิกอนบนแท่งนาโนทังสเตนไตรออกไซด์ได้รับการศึกษาโดย
การเปลี่ยนแปลงกำลังไฟฟ้าเข้าที่ใช้กับแกนสปัตเตอร์ของซิลิกอน และฟิล์มแท่งนาโนถูกสร้างขึ้นที่มุม
เหลือบ 85 องศาจากนั้น ฟิล์มจะถูกเผาที่อุณหภูมิ 400 °C เป็นเวลา 4 ชั่วโมงในอากาศ โครงสร้าง
จุลภาคและเฟสของวัสดุที่มีลักษณะเฉพาะถูกศึกษาด้วยเทคนิคเอ็กซ์เรย์โฟโตอิเล็กตรอนสเปกโทร
สโกปี การเลี้ยวเบนของรังสีเอกซ์ และกล้องจุลทรรศน์อิเล็กตรอนแบบส่องกราดการแผ่รังสีภาคสนาม
จากผลการศึกษาการตรวจจับก๊าซ พบว่าฟิล์มแท่งนาโนทังสเตนไตรออกไซด์เจือซิลิกอนในอัตราส่วน
ร้อยละ 1.43 โดยน้ำหนักมีการตอบสนองสูงสุดต่อก๊าซอะซิโตน ด้วยค่าการตอบสนอง 5.92 ที่ความ
เข้มข้น 100 ppm ณ อุณหภูมิการทำงานที่ 350 องศาเซลเซียส นอกจากนี้ผลการทดลองยังแสดงให้
เห็นถึงศักยภาพของเซนเซอร์ก๊าซอะซิโตนที่มีความไวสูงที่ความเข้มข้นต่ำ และอาจใช้เป็นเครื่องมือที่มี
ประสิทธิภาพสำหรับการตรวจสอบแบบไม่รุกรานของโรคเบาหวาน

สาขาวิชา <u>นวัตกรรม วิศวชีวการแพทย์</u>            ลายมือชื่อนักศึกษา_____
ปีการศึกษา <u>2564</u>                                        ลายมือชื่ออาจารย์ที่ปรึกษา_____

WARAPORN SUCHARITAKUL : DETECTION OF ACETONE USING SI DOPED WO$_3$ NANORODS BASED GAS SENSORS PREPARED BY MAGNETRON SPUTTERING FOR DIABETES DIAGNOSIS. THESIS ADVISOR : ASST. PROF. PUSIT MITSOMWANG, Ph.D., 51 PP.

Keyword: Si-doped WO$_3$/Gas sensor/Acetone

Gas sensing technology is currently applied in a variety of applications. In medical applications, gas sensors can be used for the detection of the biomarker in various diseases, metabolic disorders, diabetes mellitus, asthma, renal, liver diseases, and lung cancer. In this study, we present acetone sensing characteristics of Si-doped WO$_3$ nanorods prepared by a DC reactive magnetron co-sputtering with an oblique-angle deposition (OAD) technique. The composition of Si-doped in WO$_3$ has been studied by varying the electrical input power applied to the Si sputtered target. The nanorods film was constructed at the glancing angle of 85°. After deposition, the films were annealed at 400 °C for 4 hrs in the air. The microstructures and phases of the materials were characterized by X-ray photoelectron spectroscopy (XPS), X-ray diffraction (XRD), and field-emission scanning electron microscopy (FESEM). The results showed that 1.43 wt% Si-doped WO$_3$ thin film exhibited the maximum response of 5.92 towards 100 ppm of acetone at performing temperature (350 °C), purifying dry air carrier. The process exposed in this work demonstrated the potential of high sensitivity acetone gas sensor at low concentration and may be used as an effective tool for diabetes non-invasive monitoring.

School of <u>Biomedical Innovation Engineering</u>    Student's Signature _____

Academic Year <u>2021</u>    Advisor's Signature _Pusit Mitsomwang_

# ACKNOWLEDGEMENT

# TABLES OF CONTENTS

# TABLES OF CONTENTS (Continued)

# LIST OF TABLES

# LIST OF FIGURES

# LIST OF FIGURES (Continued)

# LIST OF ABBREVIATIONS

| | | |
|---|---|---|
| A | = | Angstrom |
| AcAc | = | Acetoacetate |
| $B$ | = | Sensitivity |
| 3HB | = | Betahydroxybutyrate |
| CVD | = | Chemical vapor deposition |
| °C | = | Degree Celsius |
| DC | = | Direct current |
| $e^-$ | = | Electron |
| eV | = | Electron Volt |
| eVs | = | Surface band bending |
| EDS, EDX | = | Energy Dispersive X-ray Spectroscopy |
| Ec | = | Conduction band energy |
| Eg | = | Energy gap |
| Es | = | Acceptor state |
| Ev | = | Valence band energy |
| EF | = | Fermi level energy |
| FDA | = | United States Federal Drug Administration |
| GC-MS | = | Gas chromatography with mass spectrometry |
| h | = | Plank's constant ($6.63 \times 10^{-34}$ Js) |
| $h^\cdot$ | = | Hole |
| hv | = | Photon energy Electron Microscopy |
| JCPDS | = | Joint Committee Powder Diffraction Standards |
| K.E. | = | Kinetic energy |
| LPAS | = | Light-addressable potentiometric sensors |
| FWHM | = | Full-width at half-maximum |
| FET | = | Field-Effect-Transistors |
| MF | = | Medium frequency |

# LIST OF ABBREVIATIONS (Continued)

| | | |
|---|---|---|
| mg | = | Milligram |
| ml | = | Milliliter |
| nm | = | Nanometer ($10^{-9}$ m) |
| $O_{(ads)}$ | = | Adsorbed oxygen species |
| $O_2^-$ | = | Superoxide ion |
| $O_2^{2-}$ | = | Peroxide ion |
| OAD | = | Oblique angle deposition |
| OGTT | = | Oral glucose tolerance test |
| PL | = | Photoluminescence |
| ppm | = | Part per million |
| ppb | = | Part per billion |
| ppt | = | Part per Trillion |
| PVD | = | Pulse vapors deposition |
| PTR-MS | = | Proton transfer reaction with mass spectrometry |
| RF | = | Radio frequency |
| RH | = | Relative humidity |
| Ra | = | Resistance of a sensor measured in dry air |
| Rg | = | Resistance of a sensor measured in the presence of a reducing gas or an oxidizing gas |
| $S$ | = | Sensor response |
| SCCM | = | Standard Cubic Centimeter per Minute |
| SE | = | Secondary electron |
| SEM | = | Scanning Electron Microscopy |
| SIFT-MS | = | Selected ion flow tube mass spectrometry |
| SMOX | = | Semiconducting Metal Oxide |
| STEM | = | Scanning Transmission Electron Microscopy |
| SSABET | = | Specific Surface Area form BET method |
| TEM | = | Transmission Electron Microscopy |
| TLVs | = | Threshold limit values |

# LIST OF ABBREVIATIONS (Continued)

| | | |
|---|---|---|
| $t_{res}$ | = | Response time |
| $t_{rec}$ | = | Recovery time |
| $t_{res}^{-1}$ | = | The response rate |
| VOCs | = | Volatile organic compounds |
| w | = | Surface depletion layer |
| WHO | = | World Health Organization |
| XRD | = | X-ray diffraction |
| XPS | = | X-ray photoelectron spectroscopy |
| $P$ | = | Density |
| $\lambda$ | = | Wavelength |
| $\Omega$ | = | Ohm |
| $\Phi$ | = | Work function |
| $\square$ | = | Electron affinity |
| $\mu g$ | = | Microgram ($10^{-6}$ g) |
| $\mu m$ | = | Micron ($10^{-6}$ meter) |

# CHAPTER 1

# INTRODUCTION

## 1.1    Background and rational

At present, the burden of diabetes has been rapidly increasing. The global prevalence of diabetes has been rising from 4.7% in 1980 to 8.5% in 2014. Over 420 million world populations are facing diabetes. Forecasting in 2030, demonstrates that more than 570 million people have been living with diabetes.(1) Diabetes is a chronic disease, caused by a deficiency of insulin secretion and insulin resistance. Diabetes patients who poorly control blood glucose led to increased risks of other diseases including heart, retinopathy, nephropathy, and neuropathy and nerve, increasing limb amputation. The current standard diabetes diagnostic method is to analyze the amount of insulin by pricking blood at the fingertips. This method is an invasive technique, very painful, expensive, and may be infected. A non-invasive method by human breath analysis became more interesting for detecting various volatile organic compounds that were a biomarker for detecting different diseases such as metabolic disorders, diabetes mellitus, asthma, renal and liver diseases, and lung cancer. Human exhaled breath contains nitrogen, oxygen, carbon dioxide, ammonia, hydrogen sulfide and other volatile organic compounds such as acetone.(2, 3) We monitored blood sugar levels in Diabetes mellitus (DM). The blood-sugar level is related to the ketone bodies which consist of acetoacetate, beta-hydroxybutyrate, and acetone.(4) Acetone level in the breath for healthy people is in the range of 0.5-0.9 ppm and above 1.25-2.5 ppm for diabetes patients.(5) The medical reports showed that 40 ppm of acetone was found in normal people who eat ketogenic diet (high cholesterol), 360 ppm in children with seizures, and 1250 ppm in poorly controlled diabetic patients with ketoacidosis status. Thus, the concentration of breath acetone below 0.9 ppm can be screening diabetes. There were several methods to measure breath acetone levels. The various techniques used to analyze acetone in the breath to diagnose diabetes such as Gas chromatography with mass spectrometry (GC-MS), Selected ion flow tube

mass spectrometry (SIFT-MS), Proton transfer reaction with mass spectrometry (PTR-MS), Light-addressable potentiometric sensors (LPAS), and Semiconductor metal oxide sensor (SMOS) measured in part per million (ppm), part per billion (ppb), and part per trillion (ppt).(6) In recent years, metal oxide semiconductor-based gas sensor is of great interest and widely used in portable acetone detection. Their advantages were a smaller size, higher sensitivity, lower cost, better reversibility, and easier operation compared to the other techniques, such as gas chromatography and mass spectrometry.(7) Therefore, many researchers have focused on the application of semiconductor metal oxide-based gas sensors in patients with diabetes. Therefore, many researchers have focused on investigation of semi conductive oxides with higher sensitivity to the acetone in patients with diabetes. the most acetone sensor have been considered as target gases while, ZnO, $SnO_2$, $In_2O_3$, $WO_3$ and CuO, NiO, $TiO_2$ represent $n$-type and $p$-type semiconductors respectively to study the influence of base materials.

In this work, we prepared Si-doped $WO_3$ nanorods by magnetron sputtering as a sensitive layer for acetone detection. The magnetron sputtering presented advantages with a homogeneous morphology, easily controlled the thickness of the films, and could be manipulated the composition of each deposited material by controlling the applied power to the sputtering sources.(8, 9) The acetone gas sensing performance has been characterized to demonstrate the potential of Si-doped $WO_3$ nanorods as a high sensitivity acetone gas sensor at low concentration and can be used as a non-invasive method for diabetes monitoring.

## 1.2 Objectives of this study

To fabrication Si-doped $WO_3$ nanorods prepared by magnetron sputtering as a sensitive layer for acetone detection on $Si/SiO_2$ substrate

## 1.3 Research hypothesis

Si-doped $WO_3$ nanorods have detection of acetone level ppm.

## 1.4    Benefits

The non-invasive technologies, more especially the microsensor breath technologies which are portable, cheap to fabricate, highly sensitive and easy to use, fast detection have potential in diabetes monitoring these advances will empower patients and the general population by providing them with personalized devices for monitoring, thus drastically reducing healthcare costs and potentially leading to significantly improved healthcare.
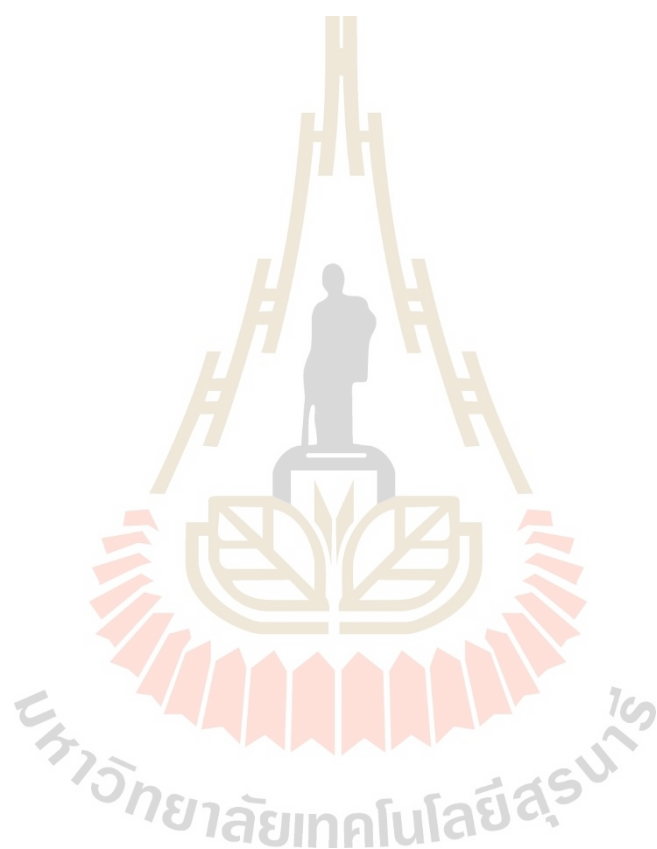
# CHAPTER 2

# THEORY AND LITERATURE REVIEWS

## 2.1 Diabetes and detection

### 2.1.1 Diabetes: Definition and diagnosis

The term diabetes describes a group of metabolic disorders characterized and identified by the presence of hyperglycemia in the absence of treatment. The pathology includes defects in insulin secretion, insulin action, or both, and disturbances of carbohydrate, fat and protein metabolism. The long-term specific effects of diabetes include retinopathy, nephropathy and neuropathy, among other complications. People with diabetes are also at increased risk of other diseases including heart, peripheral arterial and cerebrovascular disease, obesity, cataracts, erectile dysfunction, and nonalcoholic fatty liver disease. They are also at increased risk of some infectious diseases, such as tuberculosis. Diabetes may present with characteristic symptoms such as thirst, polyuria, blurring of vision, and weight loss. genital yeast infections frequently occur. The most severe clinical manifestations are ketoacidosis or a non-kenotic hyperosmolar state that may lead to dehydration, coma and, in the absence of effective treatment, death. However, in diabetic symptoms are often not severe, or may be absent, owing to the slow pace at which the hyperglycemia is worsening. As a result, in the absence of biochemical testing, hyperglycemia sufficient to cause pathological and functional changes may be present for a long time before a diagnosis is made, resulting in the presence of complications at diagnosis. It is estimated that a significant percentage of cases of diabetes (30–80%, depending on the country) are undiagnosed.

### 2.1.2 Ketone bodies in the blood

Acetone is one of the three ketone bodies found in our blood. These ketone bodies include 1)acetoacetate (AcAc), which is generated during fatty acid metabolism in the liver,2) betahydroxybutyrate (3HB), which is formed by reduction of AcAc in the mitochondria and 3)acetone, which is generated as a result of spontaneous

decarboxylation of AcAc. Acetone is an exhaled volatile organic compound that has been used as a biomarker for diabetes mellitus, especially in diabetes mellitus .It is derived from oxidation of non-esterified fatty acids, which results in acetyl-CoA and ultimately acetoacetate through spontaneous decarboxylation or enzymatic conversion.

The acetone that is produced travels through the blood and is excreted through urine, sweat and/or exhaled breath. For the exhaled breath, it has been found that the partition coefficient is 330 parts in the blood for every one part that leaves with expired air. It has been found that quantification of acetone concentration in human breath, using breath analysis techniques, correlates strongly with acetone concentration in the blood and other ketone bodies such as beta-hydroxybutyrate. Furthermore, another study by Worrall et al. has found that there is a correlation between blood glucose and volatile organic compounds. Thus, measurement of acetone from breath gives a better diagnostic control of a patient's diabetic condition rather than through the use of blood glucose measurements alone.
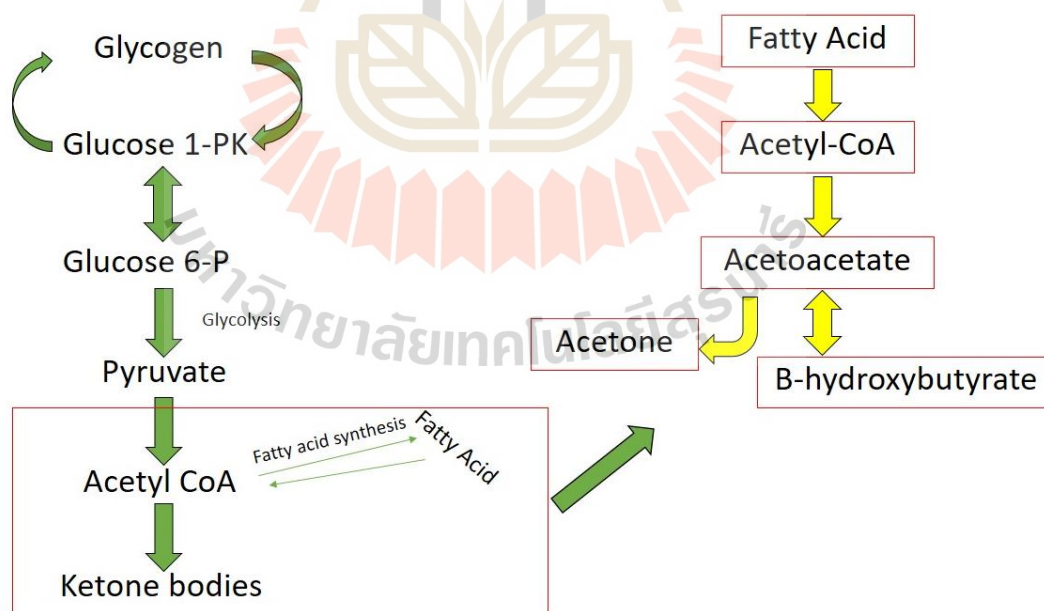
Figure 2.1 Ketone metabolism.(10)

### 2.1.3    Human Breath for Diagnosis of Diseases

Exhaled human breath consists of many kinds of chemical composition and organic substances. Some gases, including inorganic gases (e.g., NO, CO) and volatile organic compounds (VOCs, e.g., acetone, isoprene), have been considered as biomarkers for specific diseases. Acetone in the human breath, for example, is a crucial biomarker for the clinical diagnosis of diabetes. In patients with intestinal infections, hydrogen ($H_2$) and Methane ($CH_4$) can be detected from the breath and even detecting of methylmercaphen ($CH_3SH$) in patients with colon cancer and lung cancer currently, scientists are able to detect more than 300 different volatile organic compounds and other particles in breath. crucial for delivering non-invasive, real-time and rapid screening and diagnosis of complex diseases. Furthermore, it is not only non-invasive, but also has several advantages as compared to traditional diagnostic techniques, which include painless procedures and sampling that does not require skilled medical staff. Human breath contains several hundred VOCs with concentrations ranging from part-per-trillion (ppt) to part-per-million (ppm). The cellular and biochemical origin of many of these VOCs has not been determined and some of them might be of exogenous origin. Acetone level In the breath in normal people are in the range of 0.5-2.0 ppm, 1.25-2.5 ppm in patients with diabetes, 40 ppm in normal people who eat ketogenic diet (high cholesterol), 360 ppm in children with seizures, and 1250 ppm in poorly controlled diabetic patients with ketoacidosis. Therefore, acetone can act as a biomarker for metabolic (diabetes)conditions in the bloodstream. In certain cases, such as fasting, exercising and being diabetic, the liver produces ketones to act as an additional energy source, which are then metabolized into acetone and other ketone bodies. Using breath analysis techniques, acetone concentrations in exhaled breath have been shown to correlate with the acetone concentrations in the blood as well as with other ketones such as beta-hydroxybutyrate. In addition, it is also found that the level of blood glucose can be correlated to the volatile organic compound levels such as acetone.

In order to measure such low biomarker concentrations, breathing acetone is a measure of diabetes indication that requires high sensitivity, high selectivity and is a real time measurement. The technique used to analyze acetone in

the breath to diagnose diabetes is currently GC. -MS, PTR-MS, SIFT-MS, QCL, LPAS, and SMOS-base chemo resistive sensor, measured in part per million (ppm), part per billion (ppb), part per trillion (ppt).

**Table 2.1** Comparison of breath acetone analysis technique (10)

| Technique | Principle | Detection Limit | Advantages | Disadvantages |
|---|---|---|---|---|
| GC-MS | Separate and analyse compounds By MS using chromatographic column (polar or non-polar) | Ppb and ppt levels | Highly selective and sensitive | Preconcentration Steps,bulky, long sampling time,need for standards and requires trained operator |
| PTR-MS | Analyssis of ionized molecules of target analytes by reaction with $H_3O$ MS | Low ppb levels | Real-time analysis | Lack of specificity, Narrow range of detectable compounds, bulky and requires trained operator |
| SIFT-MS | Analysis of ions produced by the reaction analytes and precursor ions ($H_3O^+$,$NO^+$ or $O_2^+$) by quadrupole MS | Low ppb and ppt levels | Real-time, capability of ppt detection, broad range of detection | Cannot identify compounds bulky and require trained operator |

**Table 2.1** Comparison of breath acetone analysis technique (10) (Continued)

| Technique | Principle | Detection Limit | Advantages | Disadvantages |
|---|---|---|---|---|
| QCL | Electrons are recycled from period to period, containing each time to the gain and the photon emission | Low ppb levels | Real-time analysis potential for portability and miniaturization | Selectivity requires for practical use and currently limited by available technology to reach sufficient specificity |
| LPAS | Analysis of trace gases. It uses the Photoacoustic effect, the conversion of light to sound in all materials (solid, liquids and gases) | Ppt-ppb levels | Real time analysis | Bulky, requires trained operator |
| SMOS-based chemoresistive sensor | Measures resistivity changes based on changing in depletion layer of n-type and hole accumulation layer of p-type SMOSs around the surface when exposed to different type of gas | Ppm, ppb and ppt levels | Real time analysis, portable, inexpensive and miniaturization | Relatively low sensitivity and less selectivity |

## 2.2    Gas sensors

### 2.2.1    Performance of gas sensors

The performance of gas sensors can be evaluated by different parameters like sensitivity, selectivity, response time, reversibility or recovery time, fabrication cost and stability. An ideal sensor should possess high sensitivity, selectivity and stability, low response time and recovery time and low fabrication cost.

### 2.2.2    Types of gas sensors

1. catalytic combustion
2. electrochemical
3. thermal conductive
4. infrared absorption, paramagnetic, solid electrolyte
5. metal oxide semiconductor sensors

Moreover, classified the gas sensors based on their sensing methods and divided to two groups:

1. methods based on variation in electrical properties
2. methods based on variation in other properties. Materials like semiconductor metal oxides (SMO), carbon nanotubes and polymers are able to sense gas based on variation in electrical properties

In addition, classified the gas sensors according to the measurement methods

1. DC conductometric gas sensors
2. Field-Effect-Transistors (FET) based gas sensors
3. Photoluminescence (PL) based gas sensors

### 2.2.3    Sensor factors

**Sensitivity** is the smallest volume concentration of the target gas that can be sensed in the time of detection Sensitivity can be defined as Ra/Rg for reducing gases and Rg/Ra for oxidizing gases, where Ra is the resistance of the gas sensor in the reference gas (usually air) and Rg stands for resistance of the sensor in the target gas This is unit less parameter and percentage sensitivity is expressed by [(Ra−Rg)/Ra] * 100%

**Selectivity** is the ability of the gas sensors to detect a specific gas in a mixture of gases.

Response time is the period from the time when gas concentration reaches a specific value to that when a sensor generates a corresponding signal.

Reversibility is whether a sensor returns to its original state when gas concentration returns to normal

Recovery time is the time required for a sensor signal to return to its initial value after a step concentration change from a certain concentration value to zero.

Stability is the ability of a gas sensor to reproduce results for a certain period of time.

The result includes retaining the sensitivity, selectivity, response time and recovery time

| Parameters | Types of Gas Sensors | | | | |
|---|---|---|---|---|---|
| | SMO Gas Sensors | Catalytic Combustion Gas Sensors | Electro Chemical Gas Sensors | Thermal Conductivity Gas Sensors | Infrared Absorption Gas Sensors |
| Sensitivity | E | G | G | P | E |
| Accuracy | G | G | G | G | E |
| Selectivity | F | P | G | P | E |
| Response Time | E | G | F | G | F |
| Stability | G | G | P | G | G |
| Durability | G | G | F | G | E |
| Maintenance | E | E | G | G | F |
| Cost | E | E | G | G | F |
| Suitability to portable instruments | E | G | F | G | P |

E: excellent, G: good, F: Fair, P: Poor.

Figure 2.2 Comparison of various types of gas sensors. (11)

Semiconductor metal oxide (SMO) gas sensors are the most investigated group of gas sensors and recently the SMOs, having size in the range of 1 nm–100 nm,

are being increasingly used for gas sensing due to their size dependent properties The advantage of SMO gas sensor excellent of sensitivity, responsibility, real-time analysis, portable, inexpensive and miniaturization, good accuracy, stability, durability, fair selectivity. for fast and easy diagnosis of diabetes, there have been many researchers who have focused on the detection of the least concentration of acetone in breath. the acetone sensing performances of different semiconductor metal oxides. From most reported data, ZnO, ZnFe2O4 and Fe2O3 have been demonstrated to be the most promising potential materials for acetone sensing. (12)

| Order | Dimensions | Materials | Synthesis Method | Conc. (ppm) | LOD (ppm) | Temp. (°C) | $\tau_{res}$ (s) | $\tau_{rec}$ (s) | Resp. |
|-------|------------|-----------|------------------|-------------|-----------|------------|------------------|------------------|-------|
| 1 | | Au/ZnO nanoparticles | MOF template | 10 | 0.05 | 280 | 15 | 12 | 43 [a] |
| 2 | | $Ce/CoFe_2O_4$ nanocrystallites | molten-salt | 2000 | NA | 200 | 38 | 61 | 157 [b] |
| 3 | 0D | $Fe_2O_3$ nanoparticles | hard template | 100 | NA | 300 | 6 | NA | 26.3 [a] |
| 4 | | $Pt/In_2O_3$ nanoparticles | sol-gel | 1.56 | 0.01 | 200 | 25 | 120 | 12 [a] |
| 5 | | $ZnFe_2O_4$ nanoparticles | hydrothermal | 200 | NA | 200 | NA | NA | 39.5 [a] |
| 6 | | $LaFeO_3$ powders | sol-gel method | 10 | NA | 200 | 21 | 6 | 7.83 [b] |
| 7 | | $Co_3O_4$ nanochains | solution route | 200 | 5 | 180 | 32 | 35 | 10.5 [b] |
| 8 | 1D | $Fe_2O_3$ nanorods | interfacial-reaction | 100 | NA | 280 | 0.4 | 2.4 | 32.5 [a] |
| 9 | | $ZnFe_2O_4$ nanorods | hydrothermal | 100 | NA | 260 | 1 | 11 | 52.8 [a] |
| 10 | | $Fe_2O_3$ nanotubes | electrospinning | 100 | NA | 240 | 9 | 3 | 11 [a] |

**Figure 2.3** Summary of the gas-sensing performances of semiconductor metal oxides for acetone gas Note: Conc. = concentration; LOD = limit of detection; Temp. = temperature; $\tau$res = response time; $\tau$cov = recovery time; Resp. = Response; Ref. = References; RT = room temperature; a S = Ra/Rg; b S = Rg/Ra; c S = ($\Delta$R/Ra)*100%; d S = Ig/Ia; NA = not available.

### 2.2.4 Factors affecting the sensitivity of semiconductor metal oxide gas sensors

1. Effect of the Microstructure including grain size, number of activated adsorption sites and gas diffusion

2. Effect of the Defects

3. Effect of the Catalyst

4. Effect of the Heterojunction

5. Effect of the Humidity

### 2.2.5 Factors affecting the selectivity of semiconductor metal oxide gas sensors

Generally, two approaches exist for enhancing the selectivity of a SMO gas sensor

1. To synthesize a material which is selective to one compound and has very low or zero cross-sensitivity for other compounds which may be present in that working atmosphere.

2. Approach is to discriminate between several analytes in the mixture. This is usually achieved by either modulation of temperature or by using sensor arrays. Addition of dopants or impurities to the metal oxides or synthesis of mixed metal oxides also enhances the selectivity of the gas sensors as each material is selective to specific gas species. Dopants/impurities improve the quality and performance of the sensors

### 2.2.6 Factors affecting the stability of semiconductor metal oxide gas sensors

Stability is one of the key parameters in the development of gas sensors for the real market as the sensors should produce a stable as well as reproducible signal at least for 2–3 years which corresponds to 17,000 h–26,000 h of operation. Low stability is an issue with SMO materials. Sensor stability can be of two types. One is related to the reproducibility of the sensor characteristics during a certain period of time at working conditions including high temperature and presence of a known analyze. Such stability is referred to as active stability. The other stability is connected with retaining the sensitivity and selectivity during a period of time at normal storage conditions like room temperature and ambient humidity. According to Korotcenkov and Cho.(13) the factors which might be responsible for instability are structural transformation, phase transformation, poisoning, degradation of contacts and heaters, bulk diffusion, error in design, change in humidity, fluctuations of temperature in the surrounding atmosphere and interference effect. There is no uniform approach to increase stability of the metal oxide sensors. Stability can be increased to some extent by calcination and annealing as the post processing treatment and by reducing the

working temperature of the sensing element. Doping metal oxides with other metals or synthesis of mixed oxides also increase the stability of the sensor elements. Improvement of engineering approaches like drift compensation, selecting a correct gas system component, incorporating additional filters and temperature stabilization can also eliminate the problems of sensor stability

**2.2.7 Gas sensing mechanisms of semiconductor metal oxides**

1. Electron depletion

2. Band bending

3. Resistance change

Dopant/impurity induced enhancements of the properties of semiconductor metal oxide for gas sensing applications Doping during synthesis and deposition process influence those metal oxide properties which are important for gas sensing applications .The parameters like sensitivity, selectivity, response time and stability of the gas sensors are improved by addition of different dopants(14). There are different mechanisms which are followed by dopants/impurities to enhance the properties of nanoparticles metal oxides like

(1) change in microstructure and morphology

(2) formation of stoichiometric solid solution,

(3) change in activation energy,

(4) generating oxygen vacancy, and

(5) change in electronic structure
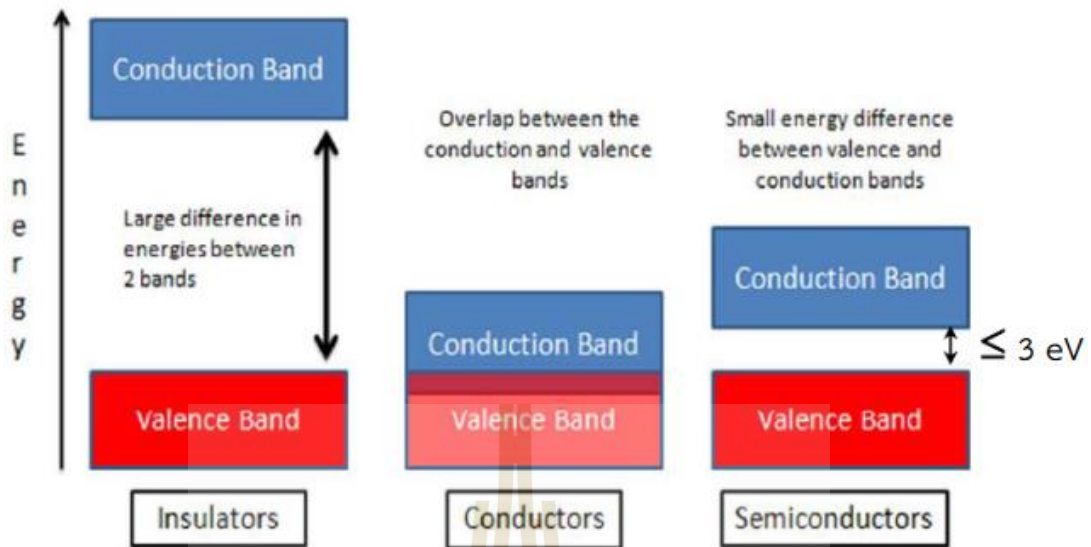
**Figure 2.4** Band Theory Applied to Sensors.

**Table 2.2** Resistance change for change in gas atmosphere. (14)

| Classification | Reducing Gas | Oxidizing Gas | Decrease in Oxygen Partial Pressure |
|---|---|---|---|
| n-type | Resistance decrease | Resistance increase | Resistance decrease |
| p-type | Resistance increase | Resistance decrease | Resistance increase |

## 2.3 Tungsten Trioxide

Tungsten trioxide ($WO_3$) is an n-type semiconductor with a band gap of 2.60 eV (Highly crystalline to 3.30 eV(amorphous) and monoclinic crystal structure. $WO_3$ is a very attractive material, because it shows a high catalytic behavior both in oxidation and reduction reactions on its surface.(15)

**Table 2.3** The crystal structure of tungsten trioxide depending on temperature.

| Crystal structure | Temperature(K) |
|---|---|
| Tetragonal | <123 |
| Orthorhombic | 123-290 |
| Monoclinic | 290-603 |
| Triclinic | 603-1013 |
| Monoclicnic | 1013 |

Recently, various chemical or physical methods have been developed successfully to synthesize nanostructured tungsten oxides, i.e. sol-gel technique, electrode position, magnetron sputtering, solution drop coating, electron beam evaporation, hot-wire CVD technique, laser-ablation technique, hydrothermal technique

**Table 2.4** Technique prepared thin film WO₃.

| Technique | Quality | Adhesion | Unifom | Repeatable | Deposition control | Large area | Environmenal toxicity |
|---|---|---|---|---|---|---|---|
| Hydrothermal | / | □ | □ | □ | □ | x | x |
| Anodize | / | / | □ | □ | □ | / | x |
| Pulsed laser deposition | / | / | / | / | / | x | x |
| Evaporation | / | □ | / | / | / | / | / |
| Sputtering | / | / | / | / | / | / | / |

Bad= x        Moderate= □        Good= /

## 2.4    Magnetron sputtering

Magnetron sputtering is a plasma coating process for metal oxide (MOX) thin film deposition whereby sputtering material is ejected due to bombardment of ions to the target surface. The vacuum chamber of the PVD coating machine is filled with an inert gas, such as argon. The argon-ions will eject sputtering materials from the target surface (sputtering), resulting in a sputtered coating layer on the products in front of the target. By applying a high voltage, a glow discharge is created, resulting in acceleration of ions to the target surface and a plasma coating There are various modes in magnetron sputtering technology including DC (direct current), MF (medium frequency), RF (radio frequency. however, there is a continuous need for developing novel materials with improved 3-S parameters (sensitivity, selectivity, stability) for gas-sensing applications. A DC potential is used to drive the ions towards the surface of one of the electrodes (the target) causing atoms to be knocked off the target and condense on the substrate surface.

A strong magnetic field is applied to contain the plasma near the surface of the target to increase the deposition rate

### 2.4.1    Glancing angle deposition (GLAD))

GLAD technique is the method to grow well ordered metal oxide nanostructures, in which a high melting point material flux is incident onto the substrate from a glancing angle, $\alpha$, in which substrate surface is rotated and tilted to an angle of greater than 80° with respect to the normal of substrate surface or less than 10° with respect to the direction of vapor flux. Low surface morbidities of ad atoms lead to kinetic limitations such as geometrical confinements and atomic shadowing, resulting in the formation of a variety of porous columnar microstructures
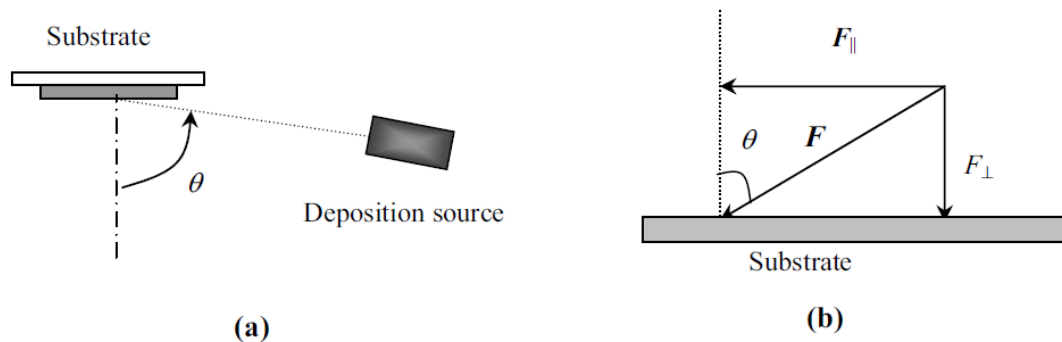
**Figure 2.5** (a) Experimental setup for oblique angle deposition; (b) The incident flux $F$ can be decomposed into two different components, $F$ is the flux perpendicular to substrate, and $F\|$ is the flux parallel to the substrate. (16)

### 2.4.2 Shadow Effect

During growth, particles can approach the surface at oblique angles and be captured by higher surface points (hills) due to the shadowing effect. This leads to the formation of rougher surfaces with columnar structures that can also be engineered to form "nanostructures" under extreme shadowing conditions, as in the case of oblique angle deposition that can produce arrays of nanorods and nano springs. Shadowing can also occur even at atomic scales (so-called "atomic shadowing effect")(17) and can cause side-wall growth of surface features during ballistic deposition of normal angle growth
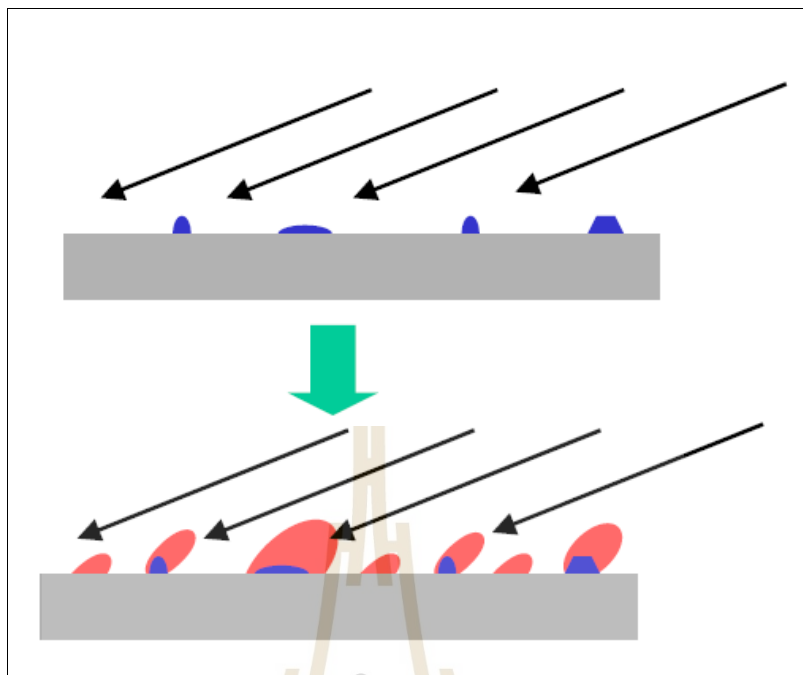
**Figure 2.6** The shadowing effect during oblique angle deposition: (a) initial nucleation
to form shadowing centers; and (b) columnar structures formed due to
the shadowing effect.

Nanomaterials are usually defined as having a particle size between 1 and 100 nanometers (nm). They are bigger than individual atoms (measured in angstroms, 1 Å = $10^{-10}$ m). The properties of nanomaterials deviate from those of "bulk" materials with the same composition, thus allowing for many interesting applications. At nano dimensions, quantum effects, like quantum confinement, permit multiple applications. Some of nanotechnology applications include alternative energy, electronics, catalysis, biomedicine, batteries, water treatment, and materials reinforcement

**Table 2.5** Metal oxides for gas-sensing applications deposited by magnetron sputtering technology. (18)

| Metal Oxide | Magnetron Sputtering Mode | Target Gases | Operating Temperature (°C) | Ref |
|---|---|---|---|---|
| CdO | DC | $NH_3$ | 150 | (19) |
| $Co_3O_4$ | RF | CO | 200 | (20) |
| CuO | DC,MF | $NO_2,C_3H_6O$ | 200,450 | (21), (22) |
| $Ga_2O_3$ | RF | $O_2$ | 1000 | (23) |
| $In_2O_3$ | RF | $CO/NO_2$ | 25 | (24), (25) |
| $MoO_3$ | DC | $H_2S$ | 280 | (26) |
| NiO | RF | $H_2,NH_3$ | 200,300 | (27), (28) |
| $Nb_2O_3$ | RF | CO | 350 | (29) |
| $TeO_2$ | RF | $NO_2$ | 90,25 | (30) |
| $SnO_2$ | RF,DC | $NO_2, NO_2$ | 60,150 | (31), (32) |
| $TiO_2$ | RF | $H_2$ | 500,25 | (33) |
| $WO_3$ | DC, RF | $C_3H_6O,CO$ | 450,200 | (34), (35) |
| $V_2O_3$ | DC | $CH_4$ | 25 | (36) |
| ZnO | RF | $H_2S,H_2$ | 250,75 | (37), (38) |
| $ZrO_2$ | RF | $O_2$ | 500 | (39) |

**Notes**: DC-direct current; MF-medium frequency; RF-radio frequency

## 2.5 Literature Reviews

### 2.5.1 Enhancement of Acetone Gas-Sensing Responses of Tapered $WO_3$ Nanorods through Sputtering Coating with a Thin $SnO_2$ Coverage Layer

Yuan-Chang Liang and Yu Chao (2019).(40) studied $WO_3$–$SnO_2$ composite nanorods were synthesized by combining hydrothermal growth of tapered tungsten trioxide (WO3) nanorods and sputter deposition of thin $SnO_2$ layers. Crystalline $SnO_2$ coverage layers with thicknesses in the range of 13–34 nm were sputter-coated onto $WO_3$nanorods by controlling the sputtering duration of the $SnO_2$. The X-ray diffraction

(XRD) analysis results demonstrated that crystalline hexagonal $WO_3$–tetragonal $SnO_2$ composite nanorods were formed. The microstructural analysis revealed that the $SnO_2$ coverage layers were in a polycrystalline feature. The elemental distribution analysis revealed that the $SnO_2$ thin layers homogeneously covered the surfaces of the hexagonally structured $WO_3$ nanorods. The $WO_3$–$SnO_2$ composite nanorods with the thinnest $SnO_2$ coverage layer showed superior gas-sensing response to 100–1000 ppm acetone vapor compared to other composite nanorods investigated in this study. The substantially improved gas-sensing responses to acetone vapor of the hexagonally structured $WO_3$ nanorods coated with he $SnO_2$ coverage layers are discussed about the thickness of $SnO_2$ coverage layers and the core-shell configuration of the $WO_3$–$SnO_2$ composite nanorods.

### 2.5.2 Effects of morphologies on acetone-sensing properties of tungsten trioxide nanocrystals

Chen et al. (2010).(41) studied triclinic $WO_3$ nanoplates and $WO_3$ nanoparticles were comparatively investigated as sensing materials to detect acetone vapors. Single-crystalline $WO_3$ nanoplates with large side-to-thickness ratios were synthesized via a topochemical conversion from tungstate-based inorganic-organic hybrid nanobelts, and the$WO_3$ nanoparticles were obtained by calcining commercial $H_2WO_4$ powders at 550 °C. The acetone-sensing properties were evaluated by measuring the change in electrical resistance of the $WO_3$ sensors before and after exposure to acetone vapors with various concentrations. The $WO_3$ nanoplate sensors showed a high and stable sensitive response to acetone vapors with a concentration range of 2–1000 ppm and the sensitivity was up to 42 for 1000ppm of acetone vapor operating at 300 °C. The response and recovery times were as short as 3–10 s and 12–13 s, respectively, for the $WO_3$ nanoplate sensors when operating at 300 °C. The acetone-sensing performance of the $WO_3$ nanoplate sensors was more excellent than that of the $WO_3$ nanoparticle sensors under a similar operating condition. The enhancement of the $WO_3$ nanoplate sensors in the acetone-sensing property was attributed to the proliferous textures, single-crystalline microstructures and high surface areas of the aggregates consisting of $WO_3$ nanoplates, which were more favorable in rapid and efficient diffusion of acetone vapors than the $WO_3$ nanoparticles.

### 2.5.3 Si: WO$_3$ Sensors for Highly Selective Detection of Acetone for Easy Diagnosis of Diabetes by Breath Analysis

Righettoni et al. (42) developed that allow rapid measurement of ultralow acetone concentrations (down to 20 ppb) with high signal-to-noise ratio in ideal (dry air) and realistic (up to 90% RH) conditions. The detector films consist of (highly sensitive) pure and Si-doped WO$_3$ nanoparticles (10–13 nm in diameter) made in the gas phase and directly deposited onto interdigitated electrodes. Their sensing properties (selectivity, the limit of detection, response, and recovery times) have been investigated as a function of operating temperature (325–500 ℃), relative humidity (RH), and interfering analyte (ethanol or water vapor) concentration It was found that Si-doping increases and stabilizes the acetone-selective Ɛ-WO$_3$ phase while increasing its thermal stability and, thus, results in superior sensing performance with an optimum at about 10 mol % Si content. Furthermore, increasing the operating temperature decreased the detector response to water vapor, and above 400 ℃, it was (≤0.7) always below the threshold (10.6) for fake diabetes detection in ideal conditions. At this temperature and 90% RH, healthy humans (≤900 ppb acetone) and diabetes patients (≥1800 ppb) can be clearly distinguished by a remarkable gap (40%) in sensor response. As a result, these solid-state detectors may offer a portable and cost-effective alternative to more bulky systems for noninvasive diabetes detection by human breath analysis.

Chaiyan et al.(43) studied the WO$_3$ nanorods were deposited by dc magnetron sputtering with GLAD technique. The structure and morphology of Au NPs decorated on WO$_3$ nanorods with varies operate pressure 10to 30 mTorr were studied. It was found that the crystal structure of all WO$_3$ nanostructure thin films exhibit amorphous due to the low energy and low mobility. Several Au nanoparticle decoration is observed to be distributed over the WO$_3$ nanorods and decreases with decoration pressure increases.

J. Krysaet al (2014).(44) studied annealing of deposited particulate WO$_3$ films at temperatures 450-500 ℃ results in better adhesion of particles to the FTO substrate and significant increase in photocurrent. Annealing at 600 ℃ caused the formation of undesirable crystal phases and a significant decrease in photocurrent.

Deposited hematite films were almost photoelectron chemically inactive but annealing in air at 650 ℃ significantly improved photocurrent; this can be explained by the diffusion of tin from the FTO substrate into hematite. Comparison of both films using irradiation AM 1.5 G. results in two times higher photocurrent for $Fe_2O_2$ film (at 1.7 V vs. RHE) but, on the other hand, the $WO_3$ film exhibits photocurrent already at 1 V (vs. RHE) where photocurrent at the $Fe_2O_3$ film is negligible

### 2.5.4 Metal Oxide Semiconductor-based gas sensor for Acetone sensing

Khodkumbhe et al.(45) studied Pristine $WO_3$ thin film-based gas sensor is a good candidate for Acetone sensing. The compact size and portability of this sensor help in easy gas sensing. The average response time of the gas sensor is calculated as 2 min. and the average recovery time is calculated to be 2.94 min. which are satisfactory for the gas sensing purpose. The response time, as well as recovery time, is found to be a minimum at 300 ℃. This ensures the efficient operation of the sensor at 300 ℃. The response is found to increase with an increase in concentration. The calibration curve has been plotted for the sensor at 300 ℃ in the range 10 ppm to 300 ppm and it can be used to know the concentration of Acetone in the air successfully for any given response in the above range. The linearity of the calibration curve makes it easy to predict the concentration of acetone.

### 2.5.5 Performance of Si-doped $WO_3$ thin films for acetone sensing prepared by glancing angle DC magnetron sputtering

Rydosz et al.(46) studied study presents the acetone sensing characteristics of Si-doped (1.0 at.%) tungsten oxide thin films prepared by glancing angle DC magnetron sputtering. The performance of Si-doped $WO_3$ sensors in the concentration range of 0.04 – 3.8 ppm at operating temperatures of 150 – 425 ℃ has been investigated. Doping of the tungsten oxide film with *Si* significantly decreases the limit of detection of acetone compared to the pure $WO_3$ sensors reported in literature. The gas sensor's response (*S*) to acetone was defined as the resistance ratio *S* =R air/R gas, where R air and R gas are the electrical resistances for the sensor in air and in gas, respectively. The maximum response measured in this experiment was S=40.5. Such response was measured in the presence of 3.8 ppm of acetone at operating temperature 425℃ using a Si-doped (1.0 at.%) $WO_3$ thin film deposited at 300℃ and

annealed at 300℃ for 4 h in air. The films phase composition, microstructure and surface topography have been assessed by XRD, SEM, AFM and EDX methods

### 2.5.6 Selective acetone gas sensors using porous $WO_3$-$Cr_2O_3$ thin films prepared by sol-gel method, Thin Solid Films

Gao et al.(47) have reported acetone gas sensors based on porous $WO_3$-$Cr_2O_3$ thin films prepared by a sol-gel method. The obtained gas response(S) defined as: S=R air/R gas, where R air is the film resistance in air and R gas is the resistance at a given concentration of analyte was around 2, 4, and 8.91 for 5 ppm, 10 ppm, and 20 ppm acetone concentrations, respectively. The relative humidity (RH) and operating temperature (OT) were set to: 20% and 320℃, respectively.

### 2.5.7 Sensing performance of palladium-functionalized $WO_3$ nanowires by a drop-casting method

Chavez et al.(48) have reported the palladium-functionalized WO3 nanowires obtained by a drop-coating method. The reported sensitivity for 1000 ppm acetone concentration is around 1.35 and OT has been set to 300 ℃.

**Table 2.6** Sensitivity to acetone concentrations of $WO_3$ sensor. (49)

| Acetone conc. | Sensing material | Response | Ref. |
|---|---|---|---|
| 0.32-1.8 ppm | $WO_3$ nanocrystals (sol-gel) | 1.7-4.7 | (50) |
| 100-300 ppm | $WO_3$ microspheres (hydrothermal) | 32-70 | (51) |
| 0.5-20 ppm | $WO_3$-$Cr_2O_3$ thin films (sol-gel) | 1-9 | (47) |
| 0.08-0.5 ppm | Si-doped 3 $WO_3$ nanostructures (flame-deposited) | 0.11-1.54 | (46) |
| 100 ppm | $WO_3$ nanostructures (acidification) | 7 | (52) |
| 1000 ppm | $WO_3$ nanowires (close-spaced CVD) | 1.35 | (53) |
| 50 ppm | $La_2O_3$-$WO_3$ nanoparticles (sol-gel) | 20 | (54) |
| 2-1000 ppm | $WO_3$ nanocrystals (hydrothermal) | 4-43 | (55) |
| 2-1000 ppm | $WO_3$ nanoplates (topochemical conversion) | 2-20 | (56) |
| 70-1000 ppm | Single crystalline $WO_3$ plates (hydrothermal) | 8-28 | (57) |
| 0.32-5 ppm | C-doped $WO_3$ (fiber-templating calcination) | 2-8 | (58) |

# CHAPTER 3

# EXPERIMENTAL DETAILS

## 3.1    Chemicals and instruments

**Table 3.1** Chemical, diameter and thick, and purity.

| Chemical | Diameter and Thick | Purity (%) |
|---|---|---|
| Tungsten target of | 2 inch-diameter and 0.25 inch-thick | 99.99 |
| Silicon target | 2 inch-diameter and 0.25 inch-thick | 99.99 |

**Table 3.2** Instruments and model used in this experiment.

| Instrument | Model |
|---|---|
| X-ray diffract meter (XRD) | Bruker D8 advance |
| field-emission scanning electron microscope (FESEM) | Carl Zeiss model AURIGA |
| Energy Dispersive X-Ray Spectroscopy (EDS) | Carl Zeiss model AURIGA |
| X-Ray Photoelectron Spectroscopy (XPS) | PHI5000 Versa Probe II (ULVAC-PHI Inc., Japan) |

## 3.2    Nanorods Fabrication



(a)                                    (b)
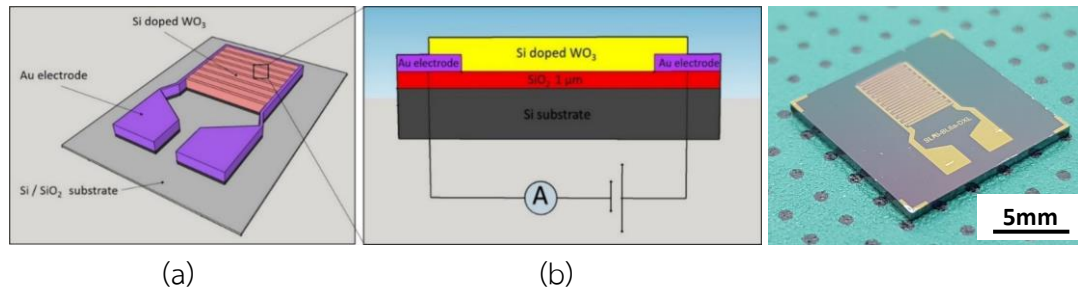
**Figure 3.1** (a) Schematic diagram of sensor design in this work (b) an optical image of
fabricated sensor.

The design of the sensor was shown in Figure 3.1(a). It consisted of a sensitive element and pairs of gold (Au) interdigitated electrodes, with interspacing between fingers of 100 $\mu$m and had an active area with approximately 3250 $\mu$m × 4000 $\mu$m, fabricated on a silicon wafer with a $SiO_2$ buffer layer. The fabrication process, after standard cleaning of Si wafer, 1 $\mu$m- thick $SiO_2$ insulating layer was grown by thermal oxidation protecting electrical connection between the substrate (Si) and the electrode. The interdigitated electrodes were patterned by photolithography and followed by lift-off of deposited 150 nm-thick Au by electron beam evaporation. Then, a sensitive layer made of $WO_3$ was deposited on top of Au interdigitated electrodes using reactive magnetron co-sputtering with oblique angle deposition (OAD) technique as described in Figure 3.2. It was used for single-step film deposition via oblique angle physical vapor deposition with precision substrate rotation. This process provides the nanorod fabrication with well dispersion .(59)
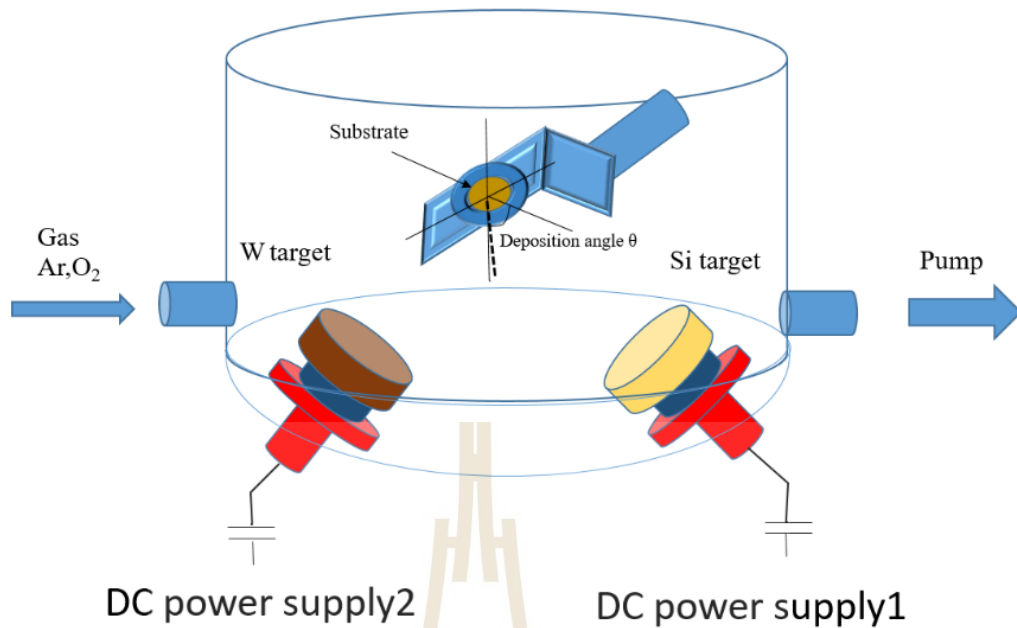
**Figure 3.2** Schematic diagram of reactive magnetron co-sputtering with OAD deposition
technique.

During the film deposition process, the nanorods could be formed on the
surface at oblique angles. Due to the shadowing effect, the particles were captured at
higher surface points (60, 61) leading to form rougher surfaces with columnar structures
as showed in Figure 3.3. In the reactive magnetron co-sputtering with OAD procedure,
nanorods were fabricated at oblique angle deposition producing arrays of nanorods
with rough surfaces. The fabricated sensor used in this work was shown in Figure 3.1(b).
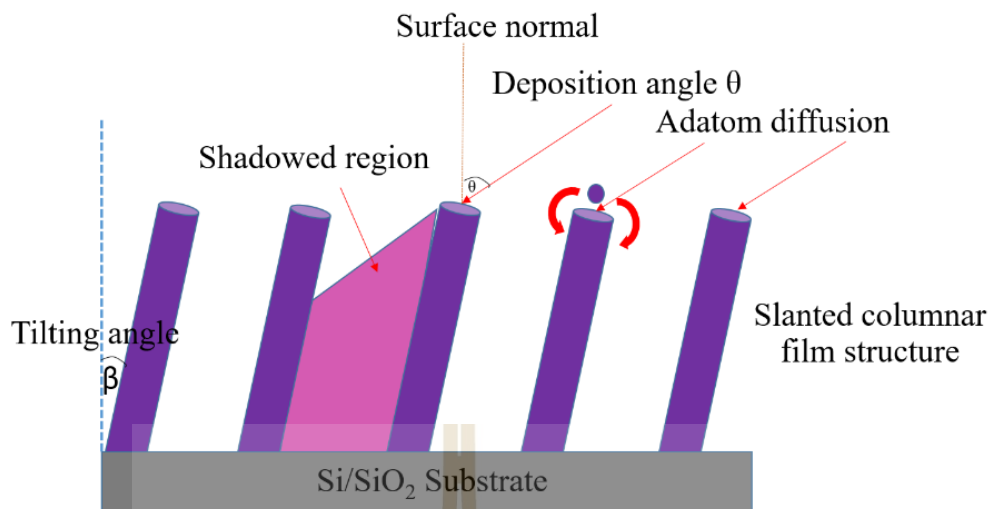
**Figure 3.3** Shadowing effect and surface diffusion and Si doped WO$_3$.

The Si-doped WO$_3$ nanorods have been deposited by reactive magnetron co-sputtering (AJA international, Inc; ATC 2000-F) with the OAD configuration. In the sputtering deposition process, the vacuum chamber was initially evacuated to a base pressure of 6.0 ×10-6 Tor. Sputtered targets made of 2-inch-diameter and 0.250-inch-thick Tungsten (99.99 % purity), and 2 inch-diameter and 0.250-inch-thick Silicon (99.99 % purity) were used as sputtered targets. Both sputtered target aligned to the center of the substrate surface in OAD geometry with the deposition angle of 85°. The W target was set at a distance of 69 mm from the centreline of the substrate. A sputtering pulse DC power of 150 W was initially applied to the tungsten target while varying input DC power from 0-30 W to silicon target. The chamber was filled with Argon (Ar) and oxygen (O$_2$) to ignite the plasma and act as a reactive gas. The Si-doped WO3 films were deposited with a constant ratio of 68% Ar/32% O2. The flows of Ar and O$_2$ were precisely controlled by mass flow controllers. The deposition pressure was maintained at 5×10$^{-3}$ Tor and the duration of deposition pressure was set at 72 min to achieve 500 nm film thickness. The sample was deposited at room temperature. Subsequently, the as-prepared samples were annealing at 400°C in the air for 4 hrs.

## 3.3 Gas-sensing measurement

The acetone gas sensing performance of Si-doped $WO_3$ nanorods was studied by using a gas sensing measurement system presented in Figure 3.4. Briefly, the target acetone concentration was achieved by mixing a clean dry air (Air zero) with an acetone gas balanced in dry air at a T-junction connector using multichannel mass flow controllers. The targeted concentration was flowed to the test chamber (2000 sccm) with flow rate of 2 L/min). The electrical resistance of the sensor was monitored using a digital electrometer. The sampling time was set to 1 s. The resistance was measured at an operating temperature ranging from 250 C° to 400 C° as a function of acetone concentration in a range from 50 ppm to 100 ppm.  The sensor response($S$) to acetone was determine as the resistance ratio $S$ = Rair/Rgas, where Rair was the resistance of the sensor in the air zero and Rgas was the resistance of the sensor upon exposure to the acetone gas. The response time is given by a time that attain 90% of the stabilized signal after gas exposure while the recovery time is defined by a time that attain 90% of the stabilized signal after air recovery.
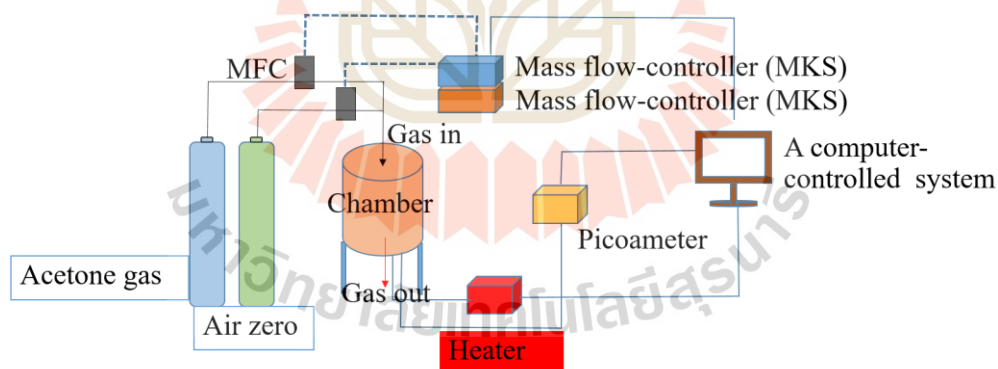


**Figure 3.4** The measurement system of sensors characteristics and gas installation.

## 3.4 Characterizations

The physical properties of the films were characterized by using an X-ray diffractometer (XRD) to point out the amorphous and crystalline states of the films. A field-emission scanning electron microscope (FESEM) was used to examine their superficial morphologies and nanostructures. The film's composition was analyzed by

using Energy Dispersive X-Ray Spectroscopy (EDS). The oxidation state of element composition was characterized by X-Ray Photoelectron Spectroscopy (XPS). The binding energy was calibrated with C 1s reference (284.8 eV).
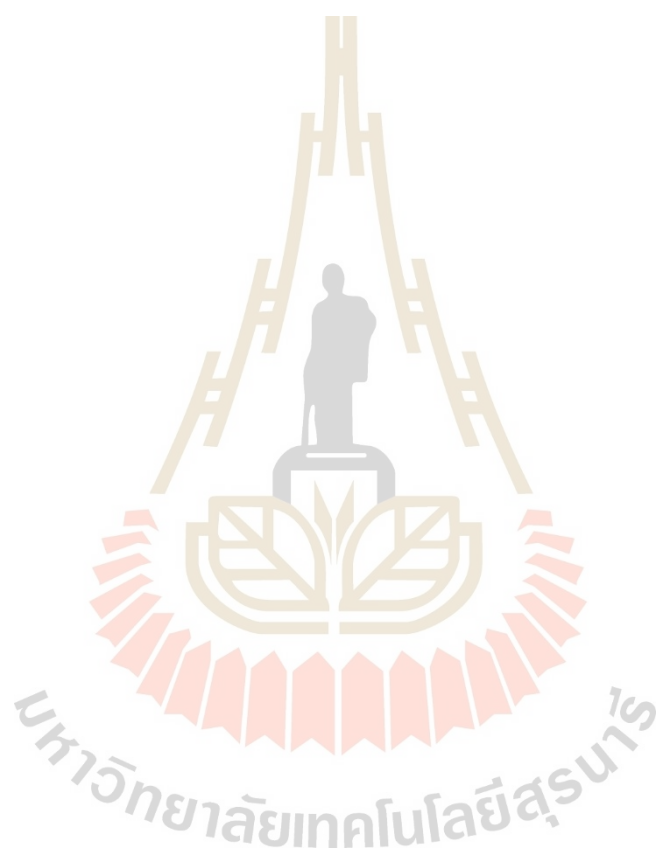
# CHAPTER 4

# RESULTS AND DISCUSSION

## 4.1 Structural and micro-morphology characterization

The XRD patterns of Si-doped $WO_3$ at different Si weight% compositions by varying the input power to Si target (5-30W) are shown in Figure 4.1. It was obvious that strong and sharp diffraction peaks were observed indicating the sample was highly crystalline. The XRD patterns of the prepared samples could be matched to a monoclinic phase of $WO_3$ (JCPDS no. 43-1035), displaying the dominant planes of (020), (200), (120) (220), (312), (140), (420) and (317) as showed in Figure 4.1. Furthermore, the XRD pattern of Si-doped $WO_3$ nanorods confirms that Si was presented in metallic Si ($Si^0$) state, which was indexed to the face centred cubic structure of Si (JCPDS no.75-0589), with the plane of (111). The appearance of the Si diffraction peaks indicate that the silicon particles may be supported on the surface of tungsten trioxide
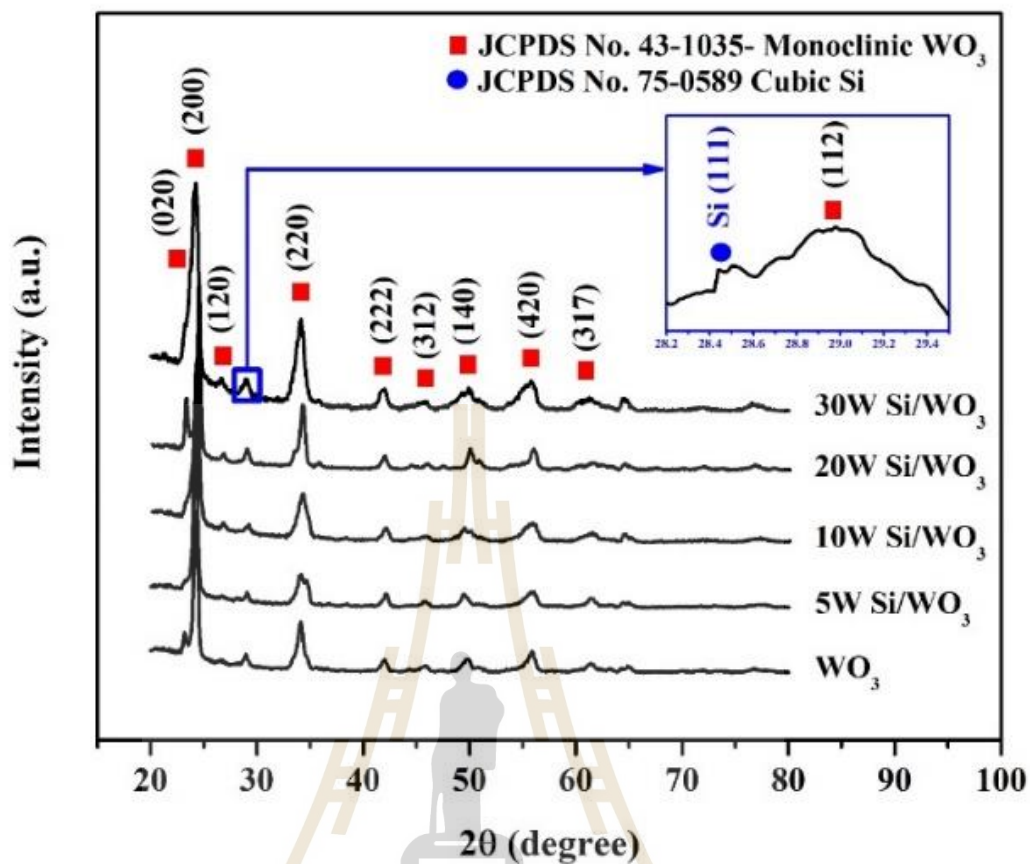
**Figure 4.1** XRD patterns of the as deposited Si doped WO$_3$ nanorods with varying the input power from 5W to 30W of Si target.

In order to verify surface morphologies and nanostructures, the composition and particularly the doping content of an obtained sample, FE-SEM and EDS were carried out as shown in Figure 4.2-4.3. Figure 4.2. shown the typical morphology and cross-section of pure and Si-doped WO$_3$ films. The SEM image of pure WO$_3$ (Figure 4.2(a)) shows that the surface contains lots of nanorods homogenously distributed on the substrate. For Si-doped WO$_3$ (Figure 4.2 (b)), some nanorods were connected. The film thickness was found to be approximately 500 nm and nanorods were deposited on the substrate with an angle of 42 degrees
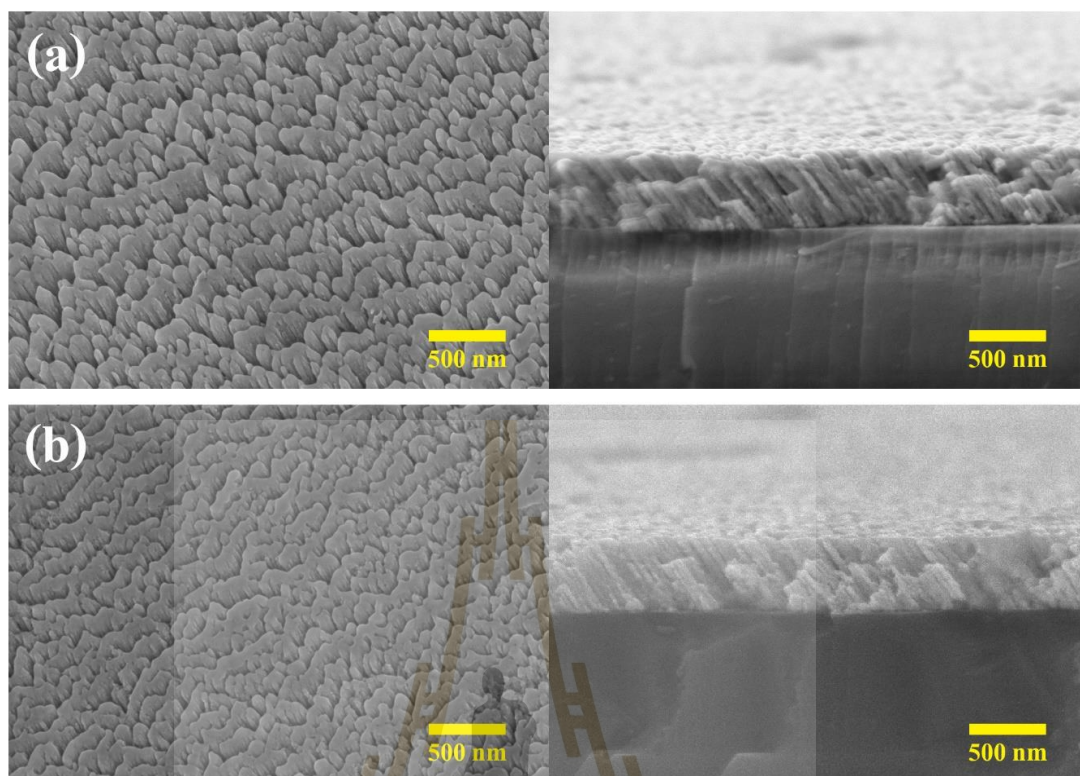
**Figure 4.2** FE-SEM surface morphology and cross section images of (a) pure $WO_3$ and
(b) Si doped $WO_3$ nanorods which deposited onto the sensor substrate after
annealing.

Figure 4.3 (a)-(e) illustrated the EDS maps and EDS spectra taken from the top-view surface morphology of Si-doped $WO_3$ (5W Si/$WO_3$ sample) after deposition and annealing at 400 °C in air. The corresponding EDS maps of W and O elements indicated homogeneous distributions of the components over the scanned region, while the distribution of Si element is visible with low intensity. The EDS spectra indicate the characteristic x-ray peaks corresponding to O, W, and Si atoms present in the sample and a small peak from C, which is derived from carbon tape used to hold the sample during the measurement. From the EDS analysis, the amount of Si was found to be 1.43 weight% (1.97 atomic%) for sample deposited input power 5 watts of Silicon target which is in good agreement with the low intensive Si distribution presented in the EDS map. The Si content tends to increase with increasing the input power of the Si source (Figure 4.3. (f))
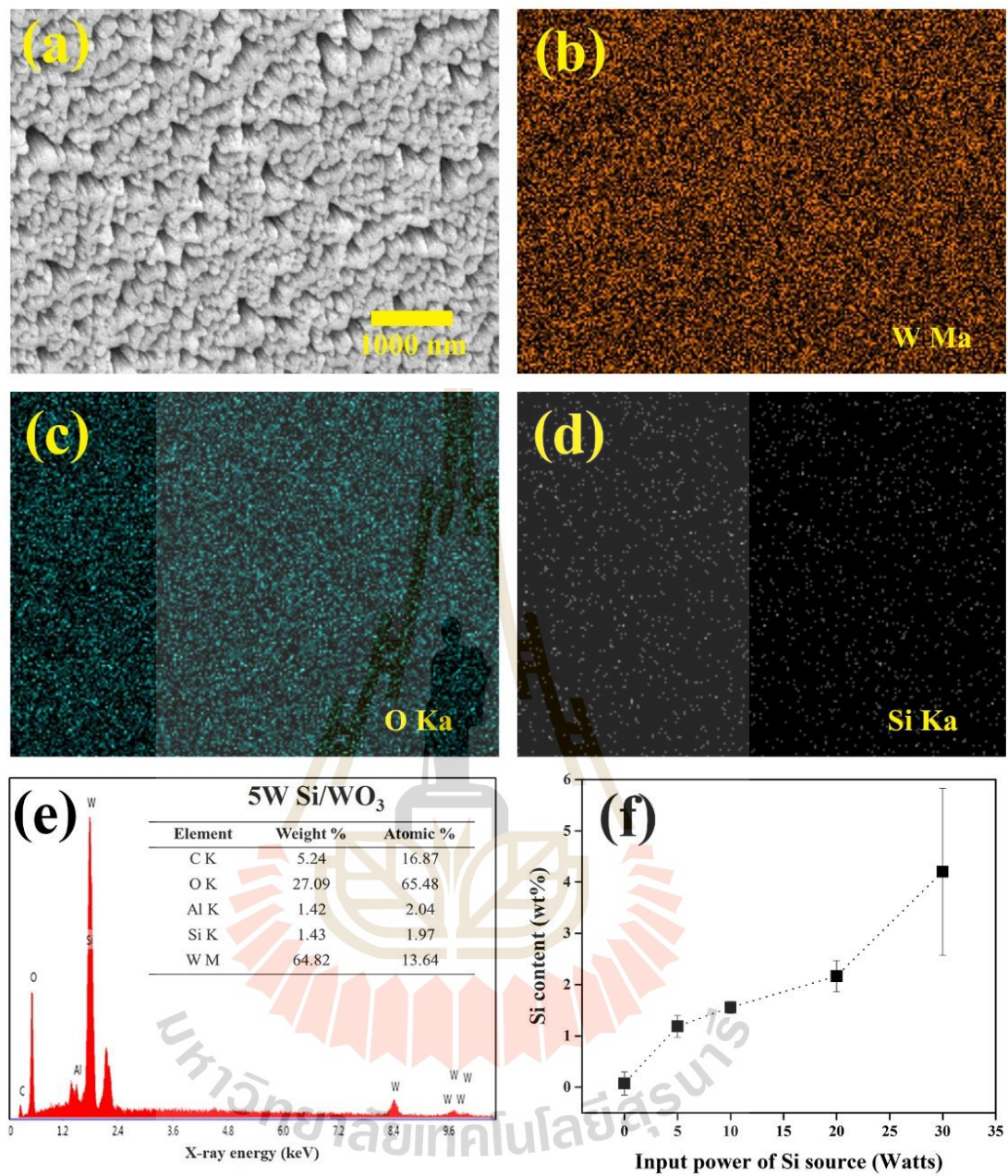
**Figure 4.3** (a) Surface morphology and EDS map showing element contribution of (b) W Ma, (c) O Ka, and (d) Si Ka and (e) EDS spectra of the 5W Si/WO₃ sample. (f) Si content (wt%) versus Input power of Si source.
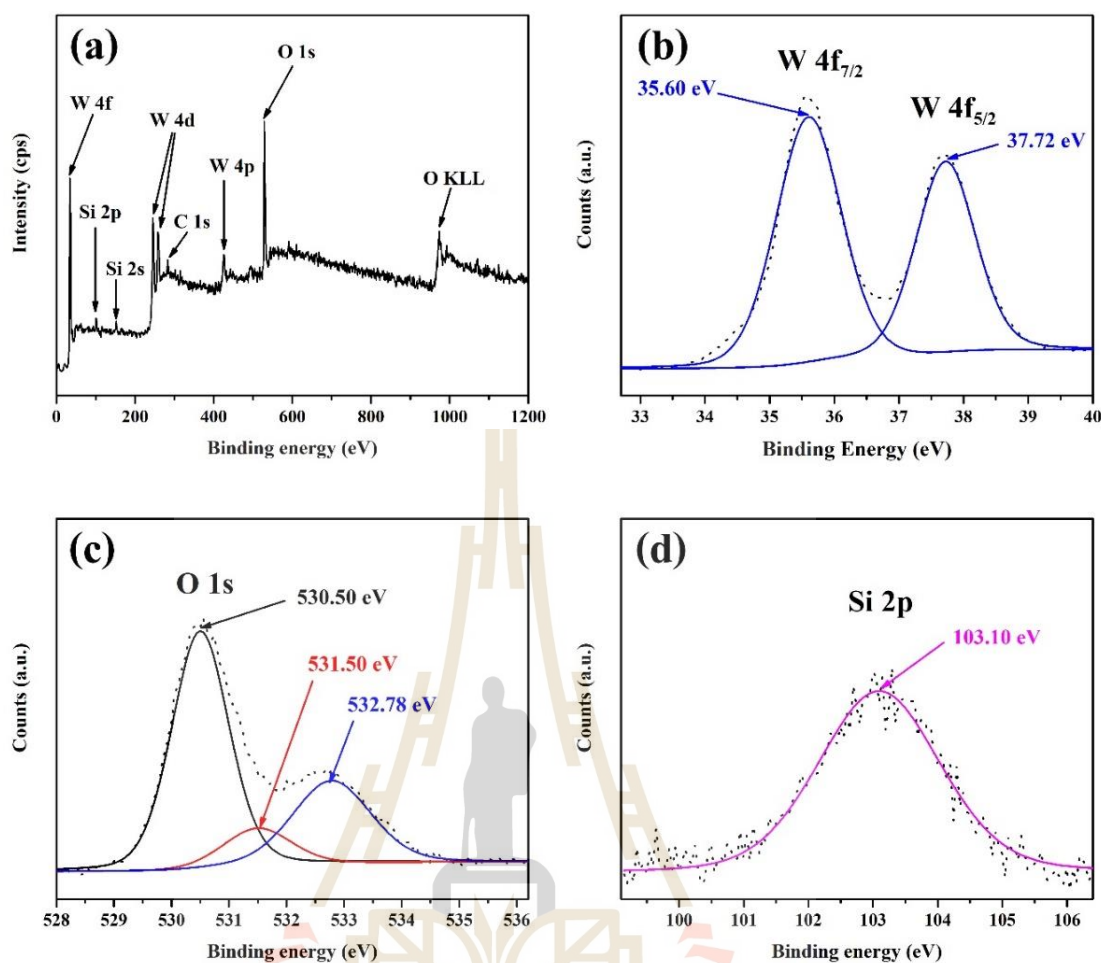
**Figure 4.4** (a) XPS survey scan spectrum and high-energy resolution core-level spectra: (b) W 4f, (c) O 1s and (d) Si 2p of 5W Si/WO$_3$ sample.

The surface chemical compositions and oxidation state of elements existing in 5W Si/WO$_3$ film after testing were illustrated in Figure 4.4. The survey scan spectrum (Figure 4.4 (a)) confirms that the expected material elements on the surface included W 4f, O 1s, and Si 2p as well as Carbon (C 1s) due to surface contamination. Considering to W 4f element (Figure 4.4 (b)), W 4f$_{7/2}$ and W 4f$_{5/2}$ core levels can be individually split into one doublet pair at binding energies of 35.60 and 37.72 eV, respectively. The binding energy difference of W 4f doublet peaks is 2.12 eV, which could be assigned to the W$^{6+}$ oxidation state.(62) For the oxygen (Figure 4.4 (c)), the curve of O 1s peak can be decomposed into three peaks located at 530.50, 531.50, and 532.78 eV. The main O 1s peak could be attributed to lattice oxygen (O$^{2-}$) while the middle and the

last ones may be associated with chemisorbed surface oxygen ($O^-$) or weakly bonded oxygen species and hydroxide species since water molecules adsorbed on the surface, respectively.(63) Regarding the Si element (Figure 4.4 (d)), the Si 2p peak was found at the binding energy of 103.10 eV, indicating that the oxidation state of Si in the sample is $Si^0$ or metallic Si. (64) Therefore, there was the presence of metallic Si distributing on the $WO_3$ surface.

## 4.2    Gas-sensing properties

The gas sensing properties were characterized using a flow-through gas sensing system. The operating temperature was an important factor influencing the surface states of the metal oxide and chemical reaction. The response of the sensors based on Si-doped $WO_3$ nanorods towards 100 ppm acetone vapour tested at different operating temperature ranging from 250-400 $^{\circ}$C are presented in Figure 4.5. It was obviously showed that the acetone response of each sensor initially increased to the highest response at an optimal temperature before decreasing when temperature increases. The optimum operating temperature for acetone gas-sensing examinations of various Si doped $WO_3$ was around 350 °C. In addition, the acetone response was sustained significantly as the small amount of Si doping but then became decreasing as the Si doping content increased at all working temperatures. Especially, Si-doped $WO_3$ sensor displays the highest response of approximately 5.92 was deposited from input power 5 watt to silicon target and co-sputtering.
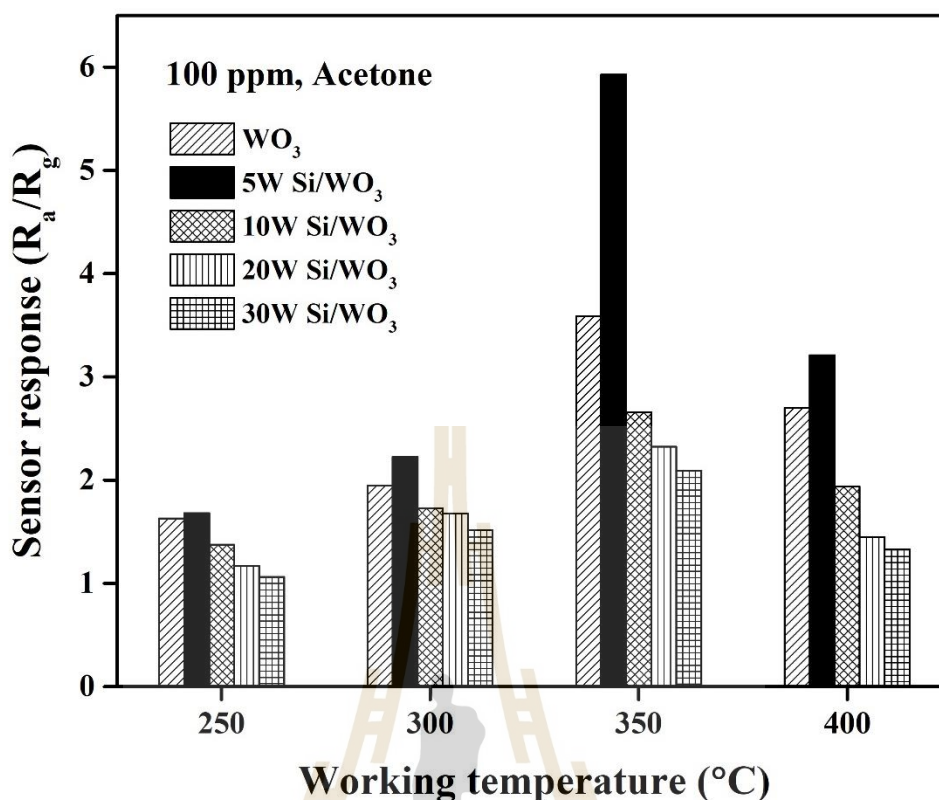
**Figure 4.5** The response of the optimal Si doped WO$_3$ nanorods in the acetone concentration of 100 ppm at difference operating temperatures.

Figure 4.6 demonstrated changes in resistance of WO$_3$ sensors with different Si doping concentrations exposed to various acetone concentrations (50-100 ppm) at the optimum working temperature. The baseline resistance of the Si-doped WO$_3$ sensor seems to decrease with increasing Si doping contents. Reduction of WO$_3$ resistance by doping Si attributes the electrons transfer at the heterojunction. The electrons are transferred from Si particles to the WO$_3$ nanorods, then electrons accumulate at the surface of WO$_3$, leading to a reduction of the baseline resistance.(65) After being subjected to acetone vapour, the resistance of all sensors decreased, especially a resistance change of Si-doped WO$_3$ sensor significantly enhanced with Si doping at 5W power of Si source before declining at the higher Si doping. It was an acetone detection at low concentration, the noise was observed during acetone exposure due to the fluctuation of acetone concentration from the bubbling process. It could be seen that the increasing response of acetone for all sensors when increasing acetone

concentration. The result implied that an increased number of acetone molecules interacted with adsorbed oxygen species on the surface of $WO_3$. Moreover, the sensor response improves substantially at the Si doping content at the 5W power source, which offers the highest acetone response of approximately 5.92 at 100 ppm. Regarding the response dependency on acetone concentration, the optimal sensor shows a low detection limit at 50 ppm with a response of around 5.20. Lastly, the acetone selectivity of the optimal sensor (5W Si/$WO_3$) was investigated against 100 ppm $H_2S$, $CO_2$, $H_2O$ and $NH_3$ at the working temperature of 350 °C, as illustrated in Figure 4.7 (a). It is seen that the sensor exhibited higher acetone response than other gases, revealing that the sensor presents the excellent acetone selectivity. Figure 4.7 (b) demonstrates the sensor response of the 5W Si/$WO_3$ sensor towards 100 ppm acetone at 350 °C for 15 days. It shows that the acetone response of the 5W Si/$WO_3$ sensor is relatively stable with fluctuation of ~20%. Therefore, Si-doped $WO_3$ sensor can be an attractive choice for acetone detection that has a great potential for breath analysis.
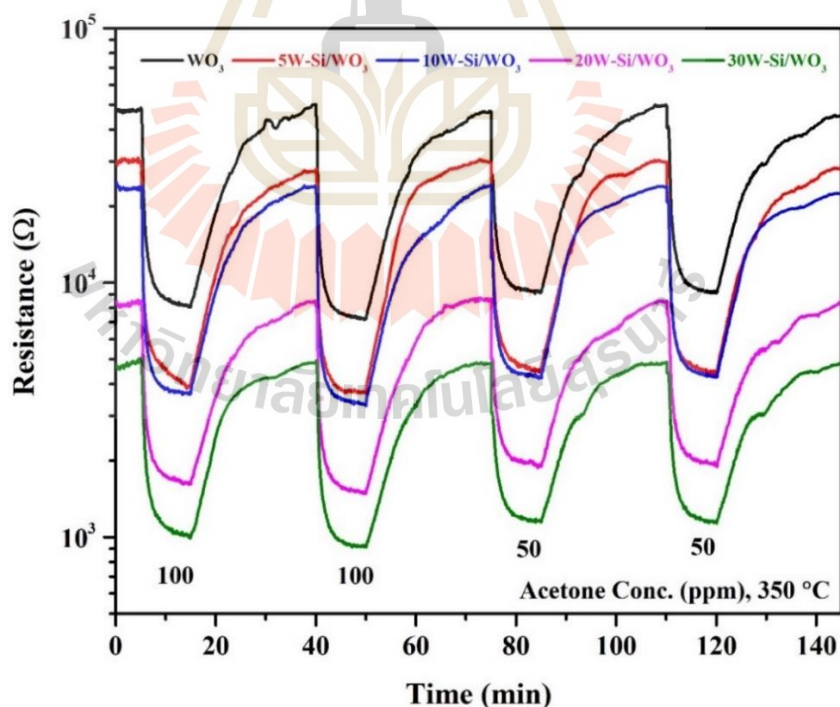


**Figure 4.6** The dynamic acetone gas-sensing response of Si doped $WO_3$ nanorods along with exposure to various acetone concentrations of 50 to 100 ppm at 350 °C.
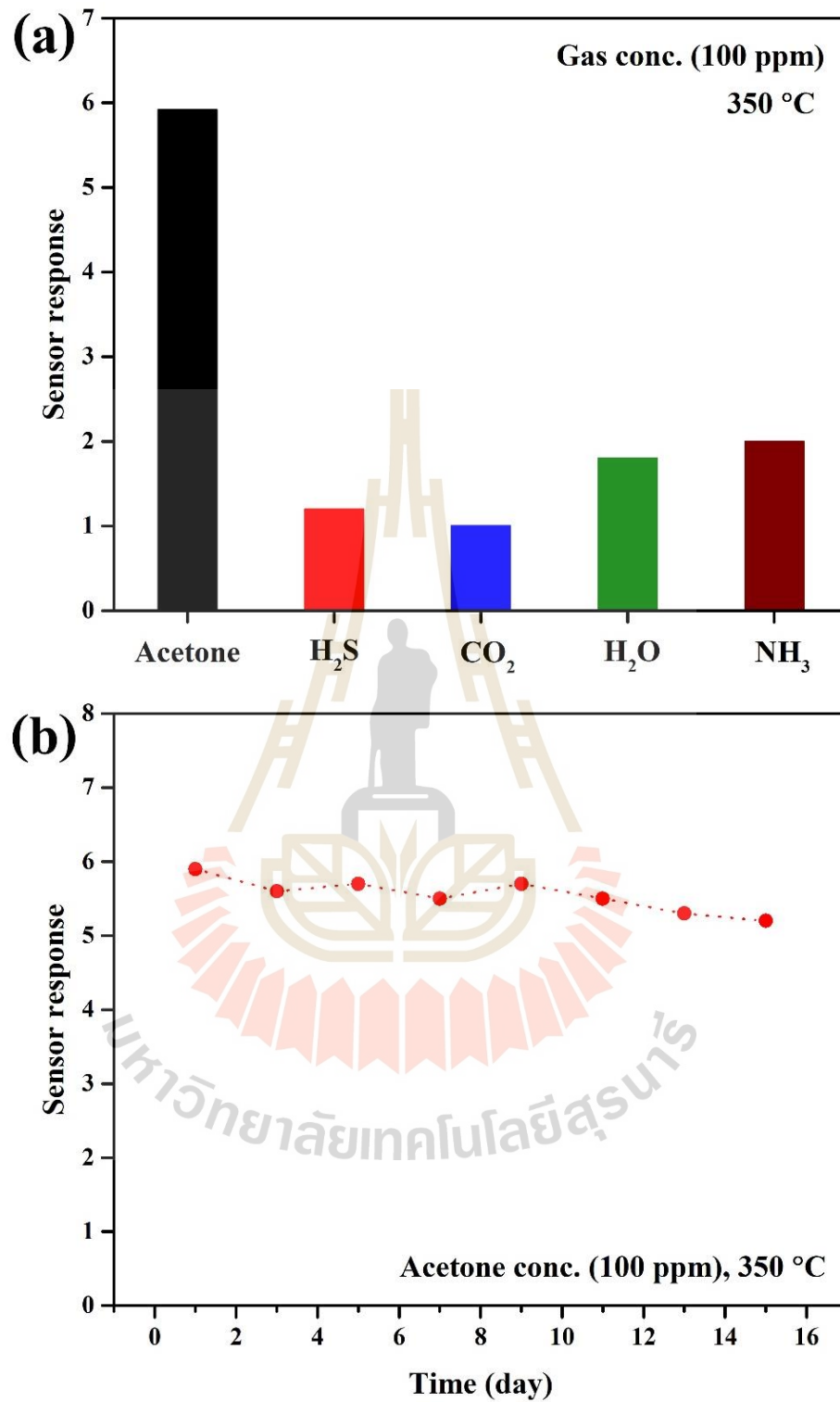
**Figure 4.7** (a) Selectivity characterization of 5W Si/WO$_3$ sensor exposed to various gases and (b) long-term stability of 5W Si/WO$_3$ sensor towards 100 ppm acetone at 350 °C.

## 4.3   Gas-sensing mechanism

The acetone gas sensitivity was investigated from the prepared Si-doped $WO_3$ nanorods at different electrical input power applied to the Si sputtered target. Mechanism of the gas sensor based on the analysis of the characteristics of above gas sensing. The sensing mechanism of Si-doped $WO_3$ nanorod-based sensor could be created by using the surface-controlled model. $WO_3$ nanorods were normally n-type semiconductors, in which electrons became the major charge carriers and played an essential role in electrical properties. Then, oxygen molecules could be easily formed chemisorbed oxygen species ($O^-$ or $O^{2-}$) (66-68) by trapping one or two electrons at the surface of $WO_3$ nanorods, which caused an increase of electron depletion region of the surface of $WO_3$ nanorods and increasing its resistance.

Under the acetone gas exposure (Figure 4.8 (a)), the acetone molecules reacted with chemisorbed oxygen partners on the surface of $WO_3$ nanorods, releasing free electron back to the $WO_3$ nanorods. Consequently, the thickness of the depletion region decreases, leading to reduction of resistance of $WO_3$ nanorods, which is good agreement with experimental result in Fig. 10. The reaction can be expressed by following Eqs. (1)-(2)(50, 69-71)

$$CH_3COCH_3 + 8O^-_{(ads)} \rightarrow 3CO_{2(g)} + 3H_2O_{(g)} + 8e^- \qquad (4.1)$$

$$CH_3COCH_3 + 8O^{2-}_{(ads)} \rightarrow 3CO_{2(g)} + 3H_2O_{(g)} + 16e^- \qquad (4.2)$$

With Si doping on the $WO_3$ nanorods, Si particles can improve acetone sensing performance in two different ways. Firstly, Si particles can be acted as catalytic for the oxygen spill-over process in Si- $WO_3$ nanorods.(71) When the air exposure to the system, Si-doped $WO_3$ nanorods can dissociate $O_2$ into $O^-$, and then $O^-$ overflow adsorbs onto the $WO_3$ surface (Figure 4.8 (b). Then Si particles reduced the activation energy required for the reaction and further enhance its response to acetone. Secondly, doping with Si can induce a large surface area. The gas response is commonly proportional to the gas-surface area interaction. (71)More and more surface-active sites by optimal Si dopants led to improve the acetone response. Therefore,

the presence of Si-doped $WO_3$ nanorods promotes additional surface-active sites and regeneration of electrons by enhancement of gas-chemisorbed oxygen interactions, leading to the overall improvement of the response.

The fast response-recovery time is greatly ascribed to more surface-active sites to promote interaction with acetone. The reactive magnetron co-sputtering with OAD technique provided the possibility for fabrication of well-ordered and sophisticated nanostructure, e.g. nanorods, nanocolumns by manipulating the deposition angle and substrate angle and fabrication Si-doped $WO_3$ nanorods prepared by magnetron sputtering as a sensitive layer for acetone detection.
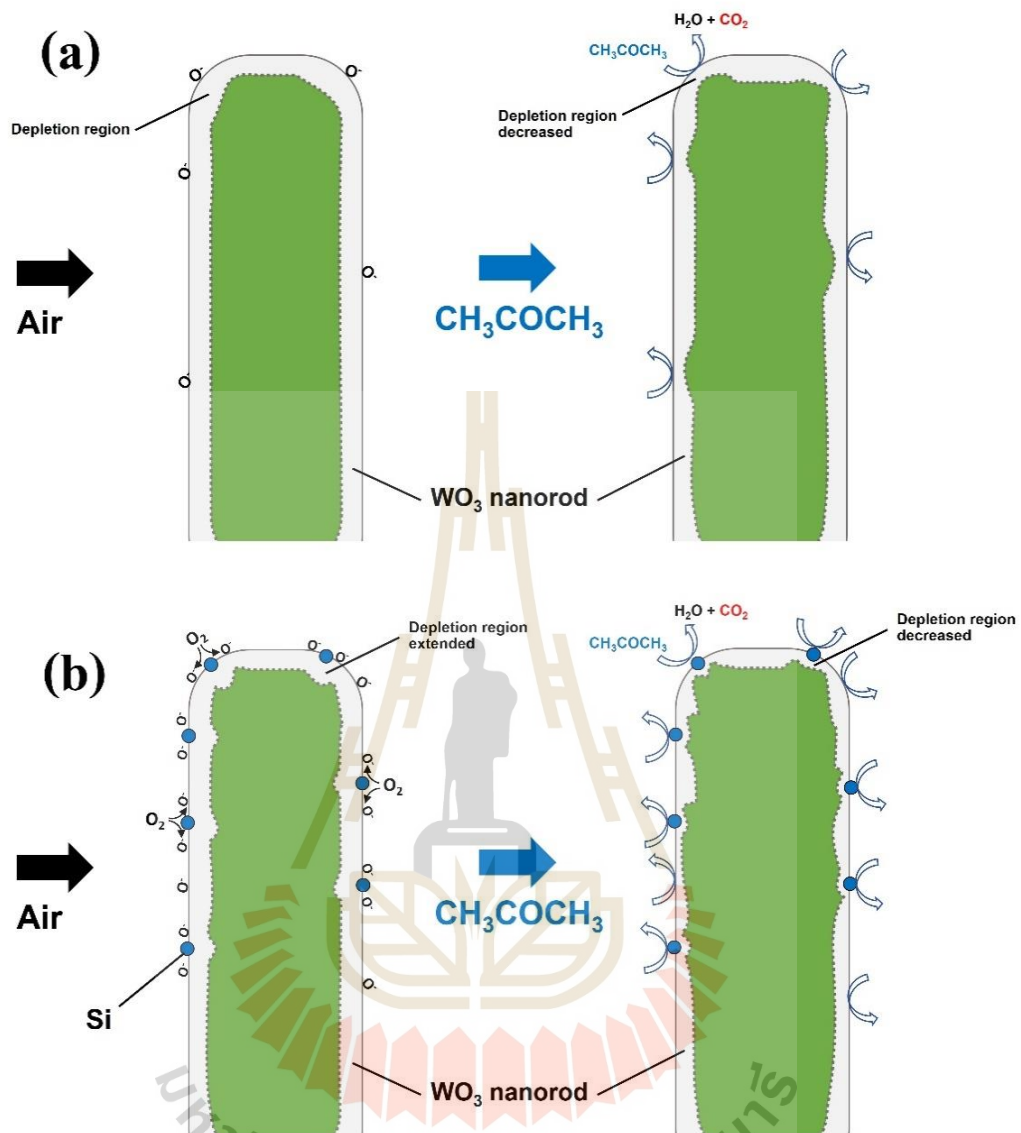
**Figure 4.8** Schematic diagram of possible gas-sensing mechanism of (a) pure $WO_3$ and (b) Si-doped $WO_3$ nanorod on exposure to acetone vapor.

# CHAPTER 5

# CONCLUSIONS

## 5.1 Silicon-doped $WO_3$ nanorods for acetone sensing application

Si-doped $WO_3$ were successfully synthesized on $Si/SiO_2$ substrate by reactive magnetron co-sputtering with OAD. After that, the films were annealed at 400 °C for 4 hrs in the air. The material characterizations demonstrated that the Si-doped $WO_3$ has shape of nanorods which deposited on the substrate with angle of 42 degree. The film thickness was found to be approximately 500 nm. The Chemical analysis results showed that Si metallic decorated on the surface of $WO_3$ nanorods.

For acetone sensing properties, 1.43% of Si-doped $WO_3$ nanorods exhibited the maximum response (S = 5.92) in the actual 100 ppm acetone at operating temperature 350 °C, purified dry air carrier. The optimal sensor had high acetone selectivity against $H_2S$, $CO_2$, $H_2O$ and $NH_3$. The improved acetone sensing mechanism contributed oxygen dissociated process on $WO_3$ and enhanced surface-active sites by Si additive. Therefore, the process exposed in this work demonstrated the potential of high sensitivity acetone gas sensor at low concentration and can be candidate for use as a supplementary tool for diabetes monitoring

## 5.2 Suggestion for future application

5.2.1 The Si-doped $WO_3$ nanorod sensor will be determine the gas-sensing characteristic could be improved by changing the thickness (looking for the optimal thickness), changing the morphology, and by adding doping, for example, Au, Pt and Pd.

5.2.2 The Si-doped $WO_3$ nanorod sensor and determine the effect of relative humidity on acetone response for apply in the exhaled breath acetone detection, to be biomarker of diabetes replace blood glucose test.

# REFERENCES

1.  Wang D. Investigation of Different Materials as Acetone Sensors for Application in Type-1 Diabetes Diagnosis. Biomedical Journal of Scientific & Technical Research. 2019;14.

2.  Wang Y, Zhou Y, Wang Y, Zhang R, Li J, Li X, et al. Conductometric room temperature ammonia sensors based on titanium dioxide nanoparticles decorated thin black phosphorus nanosheets. Sensors and Actuators B: Chemical. 2021;349:130770.

3.  Zhou Y, Wang Y, Wang Y, Li X. Humidity-Enabled Ionic Conductive Trace Carbon Dioxide Sensing of Nitrogen-Doped Ti3C2Tx MXene/Polyethyleneimine Composite Films Decorated with Reduced Graphene Oxide Nanosheets. Analytical Chemistry. 2020;92(24):16033-42.

4.  Turner C, Španěl P, Smith D. A longitudinal study of methanol in the exhaled breath of 30 healthy volunteers using selected ion flow tube mass spectrometry. SIFT-MS Physiol Meas. 2006;27:637.

5.  Anderson J, Lamm W, Hlastala M. Measuring airway exchange of endogenous acetone using a single-exhalation breathing maneuver. Journal of applied physiology. 2006;100 3:880-9.

6.  Saasa V, Malwela T, Beukes M, Mokgotho M, Liu C-P, Mwakikunga B. Sensing Technologies for Detection of Acetone in Human Breath for Diabetes Diagnosis and Monitoring. Diagnostics (Basel). 2018;8(1):12.

7.  Sun Y-F, Liu S-B, Meng F-L, Liu J-Y, Jin Z, Kong L-T, et al. Metal oxide nanostructures and their gas sensing properties: a review. Sensors (Basel). 2012;12(3):2610-31.

8.  Xu X, Yazdi MAP, Sanchez J-B, Billard A, Berger F, Martin N. Reactive co-sputtering of tungsten oxide thin films by glancing angle deposition for gas sensors. Materials Today: Proceedings. 2019;6:314-8.

9.  Bräuer G, Szyszka B, Vergöhl M, Bandorf R. Magnetron sputtering – Milestones of 30 years. Vacuum. 2010;84(12):1354-9.

10. Wang Z, Wang C. Is breath acetone a biomarker of diabetes? A historical review on breath acetone measurements. Journal of Breath Research. 2013;7(3):037109.

11. Dey A. Semiconductor metal oxide gas sensors: A review. Materials Science and Engineering: B. 2018;229:206-17.

12. Nasiri N, Clarke C. Nanostructured Chemiresistive Gas Sensors for Medical Applications. Sensors (Basel). 2019;19(3):462.

13. Korotcenkov G, Cho B. Instability of metal oxide-based conductometric gas sensors and approaches to stability improvement, G. Korotcenkov, B.K. Cho, Sens. Actuators B 156 (2011) 527-538. Sensors and Actuators B Chemical. 2011;156:527-38.

14. Lin T, Lv X, Hu Z, Xu A, Feng C. Semiconductor Metal Oxides as Chemoresistive Sensors for Detecting Volatile Organic Compounds. Sensors. 2019;19(2).

15. Shankar P, Rayappan JBB. Gas sensing mechanism of metal oxides: The role of ambient atmosphere, type of semiconductor and gases -A review. Science Letters. 2015;4:126.

16. Yiping Z, Dexian Y, Gwo-Ching W, Toh-Ming L, editors. Designing nanostructures by glancing angle deposition. ProcSPIE; 2003.

17. Xu X. Nanostructured W-O thin films by reactive sputtering : application as gas sensors Films minces d'oxydes de tungstène nano-structurés par pulvérisation réactive : application comme capteurs de gaz: Université Bourgogne Franche-Comté; 2018.

18. Rydosz A, Brudnik A, Staszek K. Metal Oxide Thin Films Prepared by Magnetron Sputtering Technology for Volatile Organic Compound Detection in the Microwave Frequency Range. Materials (Basel). 2019;12(6):877.

19. Dhivya P, Prasad AK, Sridharan M. Magnetron sputtered nanostructured cadmium oxide films for ammonia sensing. Journal of Solid State Chemistry. 2014;214:24-9.

20. Pranti AS, Loof D, Kunz S, Zielasek V, Bäumer M, Lang W. Design and Fabrication Challenges of a Highly Sensitive Thermoelectric-Based Hydrogen Gas Sensor. Micromachines (Basel). 2019;10(10):650.

21. Rydosz AM. Amorphous and Nanocrystalline Magnetron Sputtered CuO Thin Films Deposited on Low Temperature Cofired Ceramics Substrates for Gas Sensor Applications. IEEE Sensors Journal. 2014;14:1600-7.

22. Szkudlarek A, Kollbek K, Klejna S, Rydosz A. Electronic sensitization of CuO thin films by Cr-doping for enhanced gas sensor response at low detection limit. Materials Research Express. 2018;5(12):126406.

23. Ogita M, Higo K, Nakanishi Y, Hatanaka Y. Ga2O3 Thin Films for Oxygen Sensor at High Temperature. Applied Surface Science. 2001;175-176:721-5.

24. Comini E, Cristalli A, Faglia G, Sberveglieri G. Light enhanced gas sensing properties of indium oxide and tin dioxide sensors. Sensors and Actuators B-chemical - SENSOR ACTUATOR B-CHEM. 2000;65:260-3.

25. Rydosz A, Brudnik A, Staszek K. Metal Oxide Thin Films Prepared by Magnetron Sputtering Technology for Volatile Organic Compound Detection in the Microwave Frequency Range. Materials. 2019;12:877.

26. Turgut E, Coban O, Saritas S, Tuzemen S, Yildirim M, Gur E. Oxygen partial pressure effects on the RF sputtered p-type NiO hydrogen gas sensors. Applied Surface Science. 2018;435:880-5.

27. Khaniyev BA, Sagidolda Y, Dikhanbayev KK, Tileu AO, Ibraimov MK. High sensitive NH3 sensor based on electrochemically etched porous silicon. Cogent Engineering. 2020;7(1):1810880.

28. Moon HG, Jang H, Kim J-S, Park H-H, Yoon S-J. Mechanism of the Sensitivity Enhancement in TiO2 Hollow-Hemisphere Gas Sensors. Electronic Materials Letters - ELECTRON MATER LETT. 2010;6:135-9.

29. Sharma A, Tomar M, Gupta V. A low temperature operated NO2 gas sensor based on TeO2/SnO2 p-n heterointerface. Sensors and Actuators B-Chemical. 2013;176:875-83.

30. Siciliano T, Di Giulio M, Tepore M, Filippo E, Micocci G, Tepore A. Room temperature NO2 sensing properties of reactively sputtered TeO2 thin films. Sensors and Actuators B: Chemical. 2009;137:644-8.

31. Kaur M, Dadhich B, Singh R, Ganpathi K, Bagwaiya T, Bhattacharya S, et al. RF sputtered SnO2: NiO thin films as sub-ppm H2S sensor operable at room temperature. Sensors and Actuators B: Chemical. 2016;242.

32. Oros C, Horprathum M, Wisitsoraat A, Srichaiyaperk T, Samransuksamer B, Limwichean S, et al. Ultra-sensitive NO2 Sensor based on Vertically Aligned SnO2 Nanorods deposited by DC Reactive Magnetron Sputtering with Glancing Angle Deposition Technique. Sensors and Actuators B: Chemical. 2015;223.

33. Zakrzewska K, Radecka M. TiO2-SnO2 Composites and Solid Solutions for Chemical Nanosensors. Procedia Engineering. 2012;47:1077-80.

34. Rydosz AM, Szkudlarek A, Zj bka M, Domanski K, Maziarz W, Pisarkiewicz T. Performance of Si-Doped WO3 Thin Films for Acetone Sensing Prepared by Glancing Angle DC Magnetron Sputtering. IEEE Sensors Journal. 2016;16:1004-12.

35. Bose RJ, Illyasukutty N, Tan KS, Rawat RS, Matham MV, Kohler H, et al. Preparation and characterization of Pt loaded WO3 films suitable for gas sensing applications. Applied Surface Science. 2018;440:320-30.

36. Liang J, Liu J, Li W, Hu M. Preparation and room temperature methane sensing properties of platinum-decorated vanadium oxide films. Materials Research Bulletin. 2016;84:332-9.

37. Girija KG, Somasundaram K, Topkar A, Vatsa RK. Highly selective H2S gas sensor based on Cu-doped ZnO nanocrystalline films deposited by RF magnetron sputtering of powder target. Journal of Alloys and Compounds. 2016;684:15-20.

38. Bhati VS, Ranwa S, Fanetti M, Valant M, Kumar M. Efficient hydrogen sensor based on Ni-doped ZnO nanostructures by RF sputtering. Sensors and Actuators B: Chemical. 2018;255:588-97.

39. Bae JW, Park JY, Hwang SW, Yeom GY, Kim KD, Cho YA, et al. Characterization of Yttria-Stabilized Zirconia Thin Films Prepared by Radio Frequency Magnetron Sputtering for a Combustion Control Oxygen Sensor. Journal of The Electrochemical Society. 2000;147(6):2380.

40. Liang Y-C, Chao Y. Enhancement of Acetone Gas-Sensing Responses of Tapered WO3 Nanorods through Sputtering Coating with a Thin SnO2 Coverage Layer. Nanomaterials. 2019;9(6).

41. Chi X, Liu C, Liu L, Li Y, Wang Z, Bo X, et al. Tungsten trioxide nanotubes with high sensitive and selective properties to acetone. Sensors and Actuators B: Chemical. 2014;194:33–7.

42. Righettoni M, Tricoli A, Pratsinis SE. Si:WO3 Sensors for Highly Selective Detection of Acetone for Easy Diagnosis of Diabetes by Breath Analysis. Analytical Chemistry. 2010;82(9):3581-7.

43. Ahmad M, Wisitsoraat A, Zoolfakar A, ab kadir R, Wlodarski W. Investigation of RF sputtered tungsten trioxide nanorod thin film gas sensors prepared with a glancing angle deposition method toward reductive and oxidative analytes. Sensors and Actuators B: Chemical. 2014;183:364–71.

44. Cruz-Leal M, Goiz O, Chávez F, Pérez-Sánchez GF, Hernández-Como N, Santes V, et al. Study of the Thermal Annealing on Structural and Morphological Properties of High-Porosity A-WO(3) Films Synthesized by HFCVD. Nanomaterials (Basel). 2019;9(9):1298.

45. Khodkumbhe A, Nahid M, Saini V, Agarwal A, Prajesh R. Metal Oxide Semiconductor-based gas sensor for Acetone sensing. 2018 IEEE Nanotechnology Symposium (ANTS). 2018:1-4.

46. Rydosz A, Szkudlarek A, Ziabka M, Domanski K, Maziarz W, Pisarkiewicz T. Performance of Si-Doped WO3 Thin Films for Acetone Sensing Prepared by Glancing Angle DC Magnetron Sputtering. IEEE Sensors Journal. 2015;16:1-.

47. Gao P, Ji H, Zhou Y, Li X. Selective acetone gas sensors using porous WO3-Cr2O3 thin films prepared by sol-gel method. Thin Solid Films. 2012;520:3100-6.

48. Chávez F, Perez Sanchez GF, Goiz O, Zaca-Morán P, Peña-Sierra R, Morales-Acevedo A, et al. Sensing performance of palladium-functionalized WO3 nanowires by a drop-casting method. Applied Surface Science. 2013;275:28–35.

49. Rydosz A, Szkudlarek A, Zj bka M, Domanski K, Maziarz W, Pisarkiewicz T. Performance of Si-Doped WO3 Thin Films for Acetone Sensing Prepared by Glancing Angle DC Magnetron Sputtering. IEEE Sensors Journal. 2016;16:1004-12.

50. Shi J, Hu G, Sun Y, Ge M, Wu J, Liu Y, et al. WO3 nanocrystals: Synthesis and application in highly sensitive detection of acetone. Sensors and Actuators B Chemical. 2011;156:820-4.

51. Zhang Y, He W, Zhao H, Li P. Template-free to fabricate highly sensitive and selective acetone gas sensor based on WO3 microspheres. Vacuum. 2013;95:30–4.

52. Perrozzi F, Emamjomeh sm, Paolucci V, Taglieri G, Ottaviano L, Cantalini C. Thermal stability of WS2 flakes and gas sensing properties of WS2/WO3 composite to H2, NH3 and NO2. Sensors and Actuators B: Chemical. 2016;243.

53. Cruz-Leal M, Goiz O, Chávez F, Perez Sanchez GF, Hernández-Como N, Santes V, et al. Study of the Thermal Annealing on Structural and Morphological Properties of High-Porosity A-WO3 Films Synthesized by HFCVD. Nanomaterials. 2019;9:1298.

54. Luo S, Fu G, Chen H, Zhang Y. Gas sensing properties and complex impedance analysis of La2O3-added WO3 nanoparticles to VOC gases. Mater Chem Phys. 2008;109:541-6.

55. Chen D, Ge L, Yin L, Shi H, Yang D, Yang J, et al. Solvent-regulated solvothermal synthesis and morphology-dependent gas-sensing performance of low-dimensional tungsten oxide nanocrystals. Sensors and Actuators B: Chemical. 2014;205:391–400.

56. Chen D, Hou X, Li T, Yin L, Fan B, Wang H, et al. Effects of morphologies on acetone-sensing properties of tungsten trioxide nanocrystals. Sensors and Actuators B: Chemical. 2011;153:373-81.

57. Ren Y, Xie W, Li Y, Ma J, Li J, Liu Y, et al. Noble Metal Nanoparticles Decorated Metal Oxide Semiconducting Nanowire Arrays Interwoven into 3D Mesoporous Superstructures for Low-Temperature Gas Sensing. ACS Central Science. 2021;7(11):1885-97.

58. Behera B, Joshi R, Anil Vishnu GK, Bhalerao S, Pandya HJ. Electronic nose: a non-invasive technology for breath analysis of diabetes and lung cancer patients. Journal of Breath Research. 2019;13(2):024001.

59. Charles C, Martin N, Devel M, Ollitrault J, Billard A. Correlation between structural and optical properties of WO3 thin films sputter deposited by glancing angle deposition. Thin Solid Films. 2013;534:275-81.

60. Zhang J, Cao Y, Gao Q, Wu C, Yu F, Liang Y. Template-assisted nanostructure fabrication by glancing angle deposition: a molecular dynamics study. Nanoscale Research Letters. 2013;8(1):312.

61. Zhao Y, Ye D, Wang GC, Lu T-M. Designing Nanostructures by Glancing Angle Deposition. Proceedings of SPIE - The International Society for Optical Engineering. 2003;5219:59-73.

62. Liang Y-C, Chao Y. Enhancement of Acetone Gas-Sensing Responses of Tapered WO(3) Nanorods through Sputtering Coating with a Thin SnO(2) Coverage Layer. Nanomaterials (Basel). 2019;9(6):864.

63. Liang Y-C, Chang C-W. Improvement of Ethanol Gas-Sensing Responses of ZnO⁻WO(3) Composite Nanorods through Annealing Induced Local Phase Transformation. Nanomaterials (Basel). 2019;9(5):669.

64. Demchenko IN, Melikhov Y, Syryanyy Y, Zaytseva I, Konstantynov P, Chernyshova M. Effect of argon sputtering on XPS depth-profiling results of Si/Nb/Si. Journal of Electron Spectroscopy and Related Phenomena. 2018;224:17-22.

65. Li S, Yao Z, Chow G, Zhang R, Shen H. Fabrication and characterization of WO3 thin films on silicon surface by thermal evaporation. Materials Letters. 2017;195.

66. Chen D, Hou X, Li T, Yin L, Fan B, Wang H, et al. Effects of morphologies on acetone-sensing properties of tungsten trioxide nanocrystals. Sensors and Actuators B: Chemical. 2011;153(2):373-81.

67. Ren Y, Zou Y, Liu Y, Zhou X, Ma J, Zhao D, et al. Synthesis of orthogonally assembled 3D cross-stacked metal oxide semiconducting nanowires. Nature Materials. 2020;19(2):203-11.

68. Zhu Y, Zhao Y, Ma J, Cheng X, Xie J, Xu P, et al. Mesoporous Tungsten Oxides with Crystalline Framework for Highly Sensitive and Selective Detection of Foodborne Pathogens. Journal of the American Chemical Society. 2017;139(30):10365-73.

69. Chang X, Xu S, Liu S, Wang N, Sun S, Zhu X, et al. Highly sensitive acetone sensor based on WO3 nanosheets derived from WS2 nanoparticles with inorganic fullerene-like structures. Sensors and Actuators B: Chemical. 2021;343:130135.

70. Punginsang M, Wisitsoraat A, Tuantranont A, Phanichphant S, Liewhiran C. Ultrafine Bi2WO6 nanoparticles prepared by flame spray pyrolysis for selective acetone gas-sensing. Materials Science in Semiconductor Processing. 2019;90:263-75.

71. Lu W, Ding D, Xue Q, Du Y, Xiong Y, Zhang J, et al. Great enhancement of CH4 sensitivity of SnO2 based nanofibers by heterogeneous sensitization and catalytic effect. Sensors and Actuators B: Chemical. 2018;254:393-401.
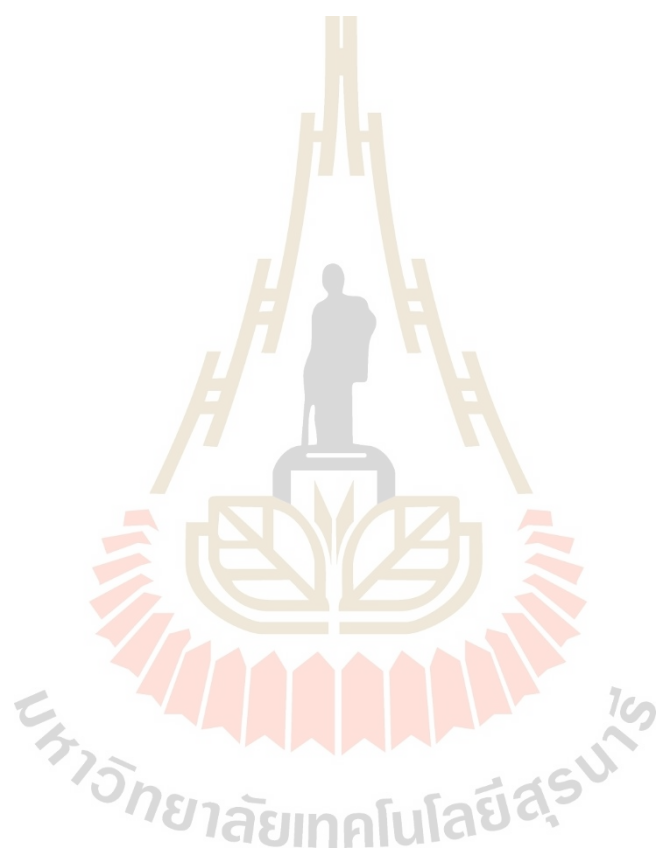
# BIOGRAPHY

Author's Name    Miss Waraporn  Sucharitakul

Date/Year of  Birth   3rd July 1983

Place of Birth    Roi-et Province, Thailand

Education     Pharm.D. (Pharm.Care), Faculty of Pharmaceutical
Science

        Khonkean University,2001-2006

        M.S. (Biomedical Innovation Engineering), Faculty of

        Engineering, Suranaree University of Technology, 2022

Experince     Pharmacist Specialist of Cardiology

        Acute care Pharmacy